Cerebral Cortex, July 2021;31: 3408–3425

doi: 10.1093/cercor/bhab020
Advance Access Publication Date: 2 March 2021
Original Article

ORIGINAL ARTICLE

Comparative Ultrastructural Analysis of Thalamocortical Innervation of the Primary Motor Cortex and Supplementary Motor Area in Control and MPTP-Treated Parkinsonian Monkeys

Rosa M. Villalba[1,2], Joseph A. Behnke[1,2], Jean-Francois Pare[1,2] and Yoland Smith[1,2,3]

[1]Division of Neuropharmacology and Neurological Diseases, Yerkes National Primate Research Center, Emory University, Atlanta, GA 30329, USA, [2]UDALL Center for Excellence for Parkinson's Disease, Emory University, Atlanta, GA 30329, USA and [3]Department of Neurology, School of Medicine, Emory University, Atlanta, GA 30329, USA

Address correspondence to Dr. Rosa M. Villalba, Yerkes National Primate Research Center, 954 Gatewood Rd NE, Emory University, Atlanta, GA 30329, USA. Email: rvillal@emory.edu.

Abstract

The synaptic organization of thalamic inputs to motor cortices remains poorly understood in primates. Thus, we compared the regional and synaptic connections of vGluT2-positive thalamocortical glutamatergic terminals in the supplementary motor area (SMA) and the primary motor cortex (M1) between control and MPTP-treated parkinsonian monkeys. In controls, vGluT2-containing fibers and terminal-like profiles invaded layer II–III and Vb of M1 and SMA. A significant reduction of vGluT2 labeling was found in layer Vb, but not in layer II–III, of parkinsonian animals, suggesting a potential thalamic denervation of deep cortical layers in parkinsonism. There was a significant difference in the pattern of synaptic connectivity in layers II–III, but not in layer Vb, between M1 and SMA of control monkeys. However, this difference was abolished in parkinsonian animals. No major difference was found in the proportion of perforated versus macular post-synaptic densities at thalamocortical synapses between control and parkinsonian monkeys in both cortical regions, except for a slight increase in the prevalence of perforated axo-dendritic synapses in the SMA of parkinsonian monkeys. Our findings suggest that disruption of the thalamic innervation of M1 and SMA may underlie pathophysiological changes of the motor thalamocortical loop in the state of parkinsonism.

Key words: electron microscopy, nonhuman primates, Parkinson's disease, thalamus, vGluT2 AB_2315569

Introduction

Our understanding of the functional circuitry of the basal ganglia-thalamo-cortical system in the normal and parkinsonian states has grown tremendously in the past decades. Functional data strongly support the notion that the communication between specific areas of the cerebral cortex and the thalamus is altered, both in Parkinson's disease (PD) patients and in animal models of parkinsonism (Wichmann and DeLong 1998, 1999, 2003, 2006, 2007; Smith et al. 1998; Turner et al. 2003; DeLong and Wichmann 2007; Pasquereau and Turner 2011; Wichmann et al. 2011; Goldberg et al. 2012; Smith et al. 2012). However, little is known about the underlying substrate of these functional changes.

In primates, the primary motor cortex (M1) and the supplementary motor area (SMA) are the main targets of the ventral motor thalamus. Although both cortical regions receive afferents from the basal ganglia– and the cerebellar-receiving

thalamus, the cerebello-thalamo-cortical system is preferentially aimed at M1, while the basal ganglia–receiving regions innervate mainly the SMA (Wiesendanger and Wiesendanger 1985; Nambu et al. 1988; Matelli et al. 1989; Darian-Smith et al. 1990; Nambu et al. 1991; Nakano et al. 1992; Darian-Smith and Darian-Smith 1993; Rouiller et al. 1994; Stepniewska et al. 1994; Inase and Tanji 1995; Shindo et al. 1995; Inase et al. 1996; Matelli and Luppino 1996; Hoover and Strick 1999; Rouiller et al. 1999; Kultas-Ilinsky et al. 2003; Morel et al. 2005; Fang et al. 2006; Stepniewska et al. 2007). In monkeys, anterograde tracing studies of thalamocortical projections from various components of the ventral motor thalamus, including the ventral anterior (VA) and ventral lateral (VL) nuclei, revealed an extensive patchy labeling in layer I, II–III, and V of M1 and SMA (McFarland and Haber 2002). A similar pattern of M1 innervation has been reported in rodents (Herkenham 1980; Ichikawa et al. 1985; Arbuthnott et al. 1990; Yamamoto et al. 1990; Castro-Alamancos and Connors 1997; Sato et al. 1997; Aumann et al. 1998; Amitai 2001; McFarland and Haber 2002; Cruikshank et al. 2007; Kuramoto et al. 2009; Rubio-Garrido et al. 2009; Hooks et al. 2013; Kaneko 2013; Kuramoto et al. 2015). In mice, projections from the basal ganglia–receiving thalamic regions terminate predominately in superficial cortical layers, while the cerebellar-receiving thalamus mostly innervates deep cortical layers (Mitchell and Cauller 2001; Kuramoto et al. 2009; Kaneko 2013; Kuramoto et al. 2015; Bopp et al. 2017). This differential laminar distribution of basal ganglia- versus cerebello-thalamocortical outflow to M1 is not as clear in monkeys (McFarland and Haber 2002). In addition to the ventral motor thalamus, the intralaminar thalamic nuclei also contribute to the innervation of motor cortices, but with a different laminar pattern of distribution. Most noticeably are the inputs from the centromedian (CM) nucleus, which target preferentially layer V of M1 in monkeys (Parent and Parent 2005).

Classical models of the basal ganglia circuitry proposed that cortical motor areas become hypoactive in PD because of reduced thalamocortical activity in response to overinhibition from the basal ganglia output nuclei upon the ventral motor thalamus (Albin et al. 1989; DeLong 1990). However, recording and imaging studies have indicated that the situation is far more complex and variable between motor cortices. Although decreased neuronal activity has been reported in the SMA and other premotor cortices of PD patients and MPTP-treated parkinsonian monkeys (Rascol et al. 1992; Sabatini et al. 2000; Cunnington et al. 2001; Lefaucheur 2005), the results are more variable and controversial in M1 (Sabatini et al. 2000; Haslinger et al. 2001; Pelled et al. 2002; Escola et al. 2003; Seiss and Praamstra 2004; Lefaucheur 2005; Parr-Brownlie and Hyland 2005; Brown et al. 2009). On one hand, some authors reported that corticospinal, but not corticostriatal, neurons decrease their firing rate and display abnormal discharge patterns in parkinsonian monkeys (Pasquereau and Turner 2011), while others did not find any significant change in the mean firing rate of M1 neurons in parkinsonian monkeys (Doudet et al. 1990; Goldberg et al. 2002). The potential sources of these pathophysiological changes in cortical activity remain unknown.

There is strong evidence for synaptic remodeling and pruning of glutamatergic and GABAergic connections throughout the basal ganglia-thalamocortical circuitry in animal models of PD (Wichmann and DeLong 1996; Obeso et al. 2000; Day et al. 2006; Villalba and Smith 2010; Villalba et al. 2015; Xu et al. 2017; Melief et al. 2018; Villalba and Smith 2018; Mallet et al. 2019; Chu 2020; Swain et al. 2020). In cortical areas of PD patients, there is a selective loss of pyramidal neurons in premotor areas (MacDonald and Halliday 2002). A major pruning of dendritic spines on layer V pyramidal neurons in M1 and dorsolateral prefrontal cortex has also been described in MPTP-treated parkinsonian monkeys (Elsworth et al. 2013; Smith et al. 2013). Whether these changes in spine density reflect a primary cortical pathology or a neuroplastic response to neuronal degeneration in the CM nucleus of MPTP-treated parkinsonian monkeys (Smith et al. 2013; Villalba, Wichmann, et al. 2014a; Villalba et al. 2019) and PD patients (Henderson et al. 2000a, 2000b; Halliday 2009) remains unclear. Either way, these neuropathological changes could lead to the breakdown and reorganization of the thalamocortical system in the parkinsonian state (DeLong 1990; Wichmann and DeLong 1996; Smith et al. 1998; Obeso et al. 2000; Escola et al. 2003; Wichmann and Delong 2007; Obeso et al. 2008; Smith et al. 2009; Wichmann and Dostrovsky 2011; Lindenbach and Bishop 2013; Taniwaki et al. 2013; Galvan et al. 2015; Pasquereau et al. 2016; Schirinzi et al. 2016; van Nuland et al. 2020).

To further address possible changes in the synaptic organization of the thalamocortical projections to motor cortices in the parkinsonian state, we used morphological and ultrastructural approaches to compare the overall pattern of synaptic connections of vGluT2-positive thalamic terminals in the superficial (II–III) and deep (Vb) layers of M1 and SMA, between control and MPTP-treated parkinsonian monkeys. The results of this analysis will compare the architecture of the thalamocortical synaptic networks between M1 and SMA of normal monkeys and determine whether these relationships are altered in the parkinsonian state.

Findings of these studies have been presented in abstract forms (Villalba, Pare, et al. 2014b; Villalba et al. 2018; Behnke et al. 2017).

Material and Methods

Animals

Brain sections from a total 6 control and 6 MPTP-treated adult male and female rhesus monkeys (*Macaca mulatta*) raised in the breeding colony of the Yerkes National Primate Research Center were used in this study (Table 1 and Supplementary Table 1). The housing, feeding, and experimental conditions used in these studies followed the guidelines by the National Institutes of Health and were approved by Emory University's Institutional Animal Care and Use Committee (IACUC).

MPTP Administration and Parkinsonism

Monkeys received systemic injections of MPTP (Sigma-Aldrich) (Supplementary Table 1). During the MPTP treatment, behavioral changes and parkinsonian motor signs were measured with quantitative methods that are routinely used in our laboratory (Altar et al. 1986; Singer et al. 1988; Herkenham et al. 1991; Johannessen 1991; Przedborski et al. 2000; Raju et al. 2008; Masilamoni et al. 2010; Villalba and Smith 2011; Mathai et al. 2015; Masilamoni and Smith 2018). Briefly, animals were transferred to an observation cage equipped with eight infrared beams arranged in a square formation on the back and one side of the cage. A computer system was attached and logged the timing of beam crossings (Banner Engineering Corp.). In addition, the animal's spontaneous behavior was videotaped, and a computer-assisted observation method was used to quantify limbs, head, and trunk movements, within a 20-min period. As

Table 1 Control and MPTP-treated monkeys used

Control			MPTP		
Monkey	Gender	Age	Monkey	Gender	Age
Primary motor cortex (M1)					
MR194	Female	13 years, 2 months	MR183	Female	17 years, 5 months
MR197	Female	2 years, 7 months	MR205	Female	14 years, 4 months
MR212	Male	10 years, 8 months	MR210	Female	13 years, 7 months
Supplementary motor area (SMA)					
MR249	Male	1 years, 9 months	MR241	Female	6 years, 10 months
MR252	Female	3 years, 9 months	MR242	Female	6 years, 9 months
MR256	Male	2 years, 1 months	MR258	Male	6 years, 11 months

in our previous studies (Raju et al. 2008; Masilamoni et al. 2010; Villalba and Smith 2011; Mathai et al. 2015; Masilamoni and Smith 2018), the video records were also used to score parkinsonian motor signs with a rating scale similar to that described by (Watanabe et al. 2005). This scale assesses key parkinsonian motor signs including gross motor activity, balance, posture, bradykinesia, and hypokinesia. Based on these behavioral scores (Supplementary Table 1), all MPTP-treated monkeys used in this study were categorized as moderate parkinsonian. Consistent with our previous studies (Villalba et al. 2009; Masilamoni et al. 2010, 2011; Villalba and Smith 2011; Masilamoni and Smith 2018), 70–90% loss of striatal dopaminergic innervation was found in these monkeys.

Animal Perfusion and Tissue Preparation

The monkeys received an overdose of pentobarbital (100 mg/kg; i.v.) and were then perfused transcardially with cold oxygenated Ringer's solution, followed by fixative containing 4% paraformaldehyde and 0.1% glutaraldehyde in phosphate buffer (PB; 0.1 M, pH 7.4). After perfusion, the brains were removed from the skull, cut into 10- to 12-mm-thick blocks in the frontal plane and postfixed in 4% paraformaldehyde for 24–48 h. The blocks of tissue used for electron microscopy studies were stored in cold phosphate-buffered saline (PBS; 0.01 M, pH 7.4) until sectioning into 60-µm-thick coronal sections with a vibrating microtome. Blocks of tissue prepared for light microscopy were immersed in a 30% sucrose solution in PB (0.1 M, pH 7.4) for at least 1 week before being cut in 50-µm-thick coronal serial sections with a freezing microtome. Sections were collected in an antifreeze solution (1.4% NaH_2PO_4-H_2O, 2.6% Na_2HPO_4-$7H_2O$, 30% ethylene glycol, 30% glycerol dissolved in distilled water) and stored in a −20 °C freezer until further processing.

Nissl Staining and Immunostaining for vGluT2

Cortical areas (M1 and SMA) and their laminar boundaries were identified in Nissl-stained sections and then matched to corresponding sections immunostained for vGluT2, used in this study as a specific marker of glutamatergic thalamocortical projections (Fremeau et al. 2001; Herzog et al. 2001; Lacey et al. 2005; Nahmani and Erisir 2005; Kashani et al. 2007; Kubota et al. 2007; Graziano et al. 2008; Raju et al. 2008; Doig et al. 2010; Villalba and Smith 2010, 2011; Garcia-Marin et al. 2013; Villalba and Smith 2013; Oda et al. 2014; Smith et al. 2014; Kuramoto et al. 2015; Vigneault et al. 2015; Bopp et al. 2017; Villalba and Smith 2018; Villalba et al. 2019; Zheng et al. 2019).

vGluT2 Antibody

A vGluT2 polyclonal antibody (Mab Technologies, Atlanta, GA; Catalog No. VGT2-6; AB_2315569) was obtained from rabbits immunized against a peptide corresponding to amino acids 560–578 of the COOH terminus of the human vGluT2 (hvGluT2). The specificity of this vGluT2 antibody on monkey tissue was determined by western immunoblots and light microscopy preadsorption immunohistochemical analyses, as previously described (Raju et al. 2008).

Immunostaining

1. *Light Microscopy (Immunoperoxidase):* Cortical coronal sections (50 µm thick; freezing microtome) containing M1 and SMA from control and MPTP-treated parkinsonian monkeys were treated at room temperature (RT) with sodium borohydride (1% in PBS) under the hood (20 min), rinsed in PBS (4–5 times), followed by a preincubation in a solution containing 1% normal goat serum (NGS), 0.3% Triton-X-100, and 1% bovine serum albumin (BSA) in PBS. Sections were then incubated for 24 h at room temperature (RT) in a PBS solution (with 1% NGS, 0.3% Triton-X-100, and 1% bovine serum albumin-BSA) containing the primary antibody, a rabbit anti-vGluT2 antibody (dilution: 1:5000). Following the primary antibody incubation, the sections were thoroughly rinsed in PBS and incubated for 90 min at RT with a biotinylated goat anti-rabbit IgGs (Vector) diluted at 1:200 in a PBS solution containing 1% normal nonimmune serum, 0.3% Triton-X-100, and 1% BSA. This was followed by washes in PBS and a 90 min incubation at RT in the avidin–biotinylated peroxidase complex (ABC; Vector) diluted at 1:100 in the same diluents as for the primary and secondary antibodies. Finally, sections were rinsed in PBS and TRIS buffer (0.05 M, pH 7.6) before being placed in a solution containing 0.025% diaminobenzidine (3,3′-diaminobenzidine tetrahydrochloride, DAB; Sigma), 0.01 M imidazole (Fisher Scientific), and 0.005% H_2O_2 for 10 min at RT. The reaction was stopped by washes in PBS, and the sections were mounted on gelatin-coated slides, dehydrated in alcohol, immersed in toluene, and coverslipped with Permount. Finally, slides were scanned using a ScanScope CS scanning system (Aperio Technologies). Digital representations of the

slides were saved and analyzed using ImageScope software (Aperio Technologies).

2. *Electron Microscopy (Pre-embedding Immunoperoxidase):* Vibratome coronal sections (60 µm thick) including M1 and SMA were treated with a 1% sodium borohydride solution, placed in a cryoprotectant solution (PB 0.05 M; pH 7.4; 25% sucrose, and 10% glycerol), frozen at −80 °C for 20 min, thawed, and returned to a graded series of cryoprotectant solution diluted in PBS. They were then washed in PBS and preincubated for 1 h at RT in a solution containing PBS, 1% normal goat serum (NGS), and 1% bovine serum albumin (BSA), then incubated in the primary rabbit anti-vGluT2 antibody (dilution 1:5000) for 48 h at 4 °C, and their localization was revealed using the avidin–biotin–peroxidase complex method (ABC-Vectastain Standard kit, Vector Labs) with a DAB solution used as chromogen for the peroxidase reaction, as described above. Immunostained sections were postfixed in osmium tetroxide, dehydrated in alcohol and propylene oxide, embedded in resin (Durcupan, ACM, Fluka) for at least 12 h, mounted on slides, and coverslipped. The resin was polymerized at 60 °C for 48 h (Villalba et al. 2016).
3. *Control Experiments:* In a series of control experiments, sections were processed as described above, but without primary antibodies (as a control for the specificity of secondary antibodies). In these sections, there was a complete lack of immunostaining.

Measurement of vGluT2-Immunostaining Intensity in M1 and SMA

Digital images of the vGluT2-immunostained M1 and SMA cortical areas were selected using the ImageScope viewer software (Aperio). Before the intensity analysis (FIJI, NIH), each image was converted to black and white (16-bit grayscale format) and inverted to dark-field images using Adobe Photoshop (CC 2019).

Ultrathin Sectioning and Electron Microscopy Analysis

Blocks of immunostained tissue were taken from areas most enriched in vGluT2-positive terminal-like profiles of layers II–III and Vb of M1 and SMA, glued on top of resin blocks, trimmed and cut into 60-nm ultrathin serial sections with an ultramicrotome (Ultracut T2; Leica), and collected on single-slot Pioloform-coated copper grids. Areas of tissue containing large blood vessels, aggregates of myelinated axons and somas were avoided. Taking into consideration the limited access of antibodies to antigenic sites deep in the sections, ultrathin sections were obtained from the surface of each block. Ultrathin sections were stained with lead citrate for 5 min and examined with a JEOL/JEM-1011 electron microscope (see Villalba et al. 2016). The investigator collecting the electron microscope (EM) images was blinded to the animal group under study until all electron microscope data had been gathered and tabulated. All vGluT2-positive terminals (identified by the dark amorphous DAB deposit) that formed a well-differentiated synapse with dendritic spines or shafts were photographed (55–60 images per animal and cortical layer) at ×60 000 magnification with a CCD camera (DualView 300W; DigitalMicrograph software, version 2.30.542.0; Gatan, Inc.). The postsynaptic target (dendritic spine or dendritic shaft) and the postsynaptic density (PSD) morphology (macular or perforated) of the vGluT2-positive terminals were compared in superficial (II–III) and deep (Vb) layers of M1 and SMA between control and MPTP-treated parkinsonian monkeys. Spines were defined as protrusions emerging from dendritic shafts. Because data were collected from single ultrathin sections, it was not always possible to visualize the parent dendrite from which spines originated from. Thus, additional ultrastructural criteria such as the presence of the spine apparatus (stacked smooth endoplasmic reticulum) and lack of mitochondria were used to differentiate dendritic spine profiles from small dendritic shafts. According to previous studies, macular-shaped PSDs were defined as being continuous without any segmentation, while perforated-shaped PSDs were categorized by their segmented postsynaptic densities (Geinisman 1993; Neuhoff et al. 1999; Harris and Weinberg 2012; Harris 2020).

Statistical Analysis

The differences between control and MPTP-treated monkeys in M1 and SMA were statistically assessed using Student's *t*-test and interindividual difference between animals of the same group was tested using one-way ANOVA (Sigmaplot 14.0 software).

Photomicrographs Production

Light and electron microscopic micrographs shown in this manuscript were digitally acquired, imported in TIFF format to Adobe Photoshop (CC 2019; Adobe Systems), and adjusted only for brightness and contrast, to optimize the quality of the images for analysis. Micrographs were then compiled into figures using Adobe Photoshop CS6.

Results

Light Microscopy Analysis

Optical Density of vGluT2 Immunostaining in M1 and SMA

The intensity of staining was measured in sections from 2 control and 2 MPTP-treated monkeys (one section per monkey) for each of the motor areas analyzed. Measurements were collected from three ROIs that included the upper, middle, and lower dorsoventral tier of each cortical layer analyzed (II–III and Vb). The quantitative data for each ROI and the mean values for each layer are shown in the Supplementary Table 2. No significant interindividual differences (one-way ANOVA) were found between the 2 animals of the same group used for the analysis.

In M1, comparison of vGluT2-immunostaining intensity in control and MPTP-treated parkinsonian monkeys revealed a significant decrease (80–85%) in the intensity of vGluT2 immunoreactivity in deep cortical layers (layer Vb) (Student's *t*-test, $^{*}P \leq 0.001$), while a slight, not significant (Student's *t*-test, $P = 0.416$), increase (~5%) in vGluT2 labeling was found in layer II–III (Fig. 1*B*,*C*,*E*). A similar significant decrease (Student's *t*-test, $^{*}P = 0.037$) in thalamic innervation of deep cortical layers was also found in SMA (~70%), while a smaller, albeit statistically significant (Student's *t*-test, $^{*}P = 0.007$), decrease in labeling (~25%) was found in layers II–III in MPTP-treated monkeys (Fig. 1*D*,*E*,*G*).

Electron Microscopy Analysis

vGluT2-Positive Terminals

To characterize the ultrastructural features and pattern of synaptic connectivity of vGluT2-containing thalamocortical

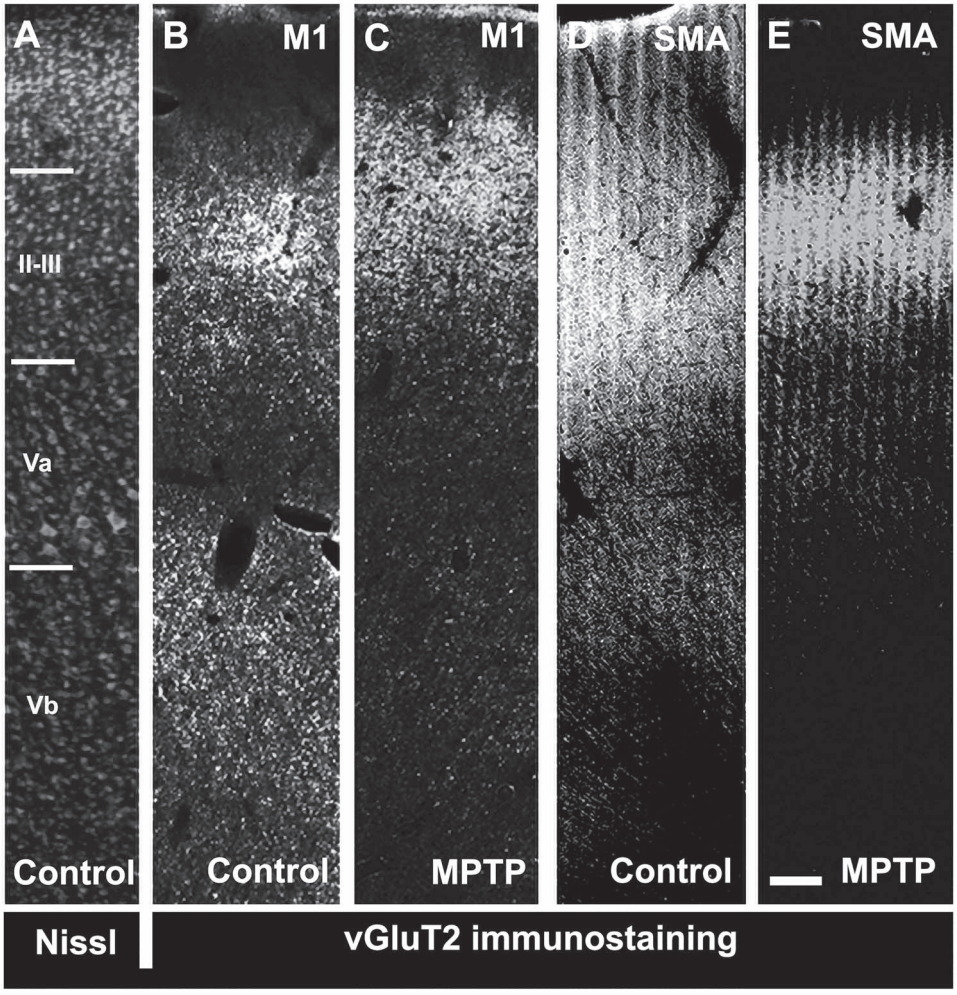

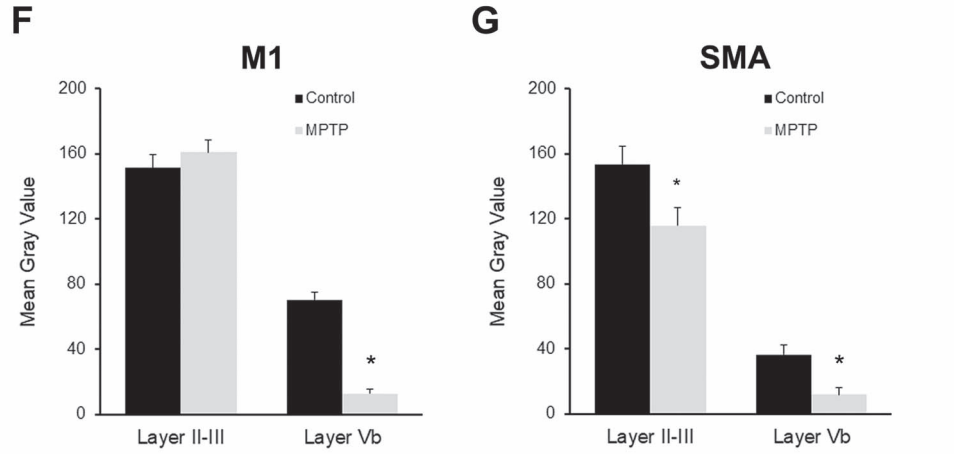

Figure 1. Light microscopy images of motor cortical areas. (*A*) Nissl-stained section (inverted to a darkfield image) showing the different cortical M1 layers. (*B–E*) Light microscopy (inverted images) of vGluT2 immunostaining in M1 (*B* and *C*) and SMA (*D* and *E*) cortex in control (*B* and *D*) and MPTP-treated (*C* and *E*) animals. (*F* and *G*) Comparison of vGluT2-immunostaining intensity (mean gray value) in M1 (*F*) and SMA (*G*) cortical layers II–III and Vb in control and MPTP-treated parkinsonian monkeys. There is a significant decrease in the intensity of vGluT2 immunoreactivity in layer Vb of M1 (80–85%; Student's *t*-test, $^{*}P \leq 0.001$) and SMA (~70%; Student's *t*-test, $^{*}P = 0.037$) in parkinsonian animals. In SMA (*G*), there is also a significant decrease in labeling in layers II–III in MPTP-treated monkeys (~25%; Student's *t*-test, $^{*}P = 0.007$). Scale bar in *E* (applies to *A–D*): 250 µm.

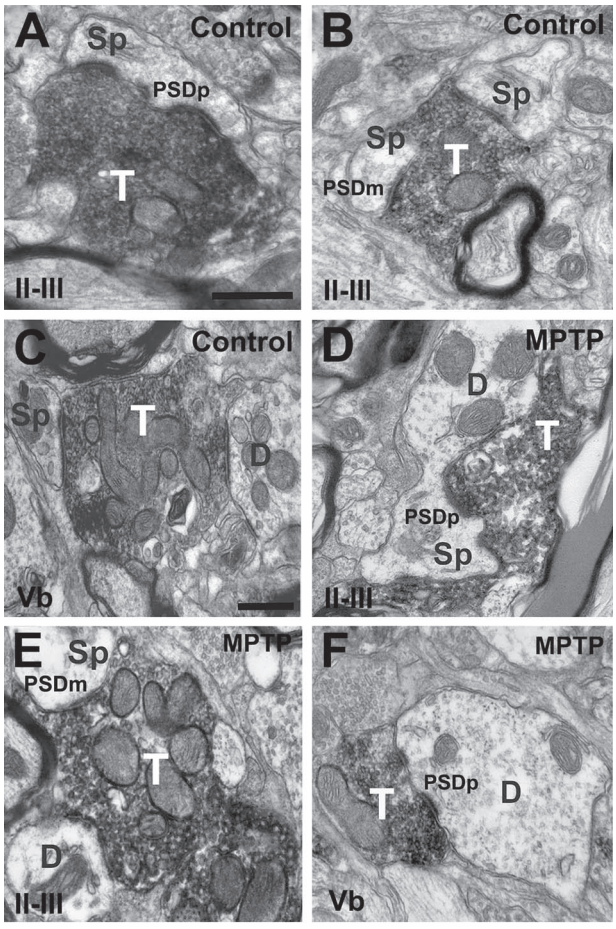

Figure 2. vGluT2-immunorecative terminals in M1. Electron micrographs of vGluT2-immunopositive terminals in layers II–III (*A*, *B* and *D*, *E*) and Layer Vb (*C*, *F*) from control (*A*–*C*) and MPTP-treated (*D*–*F*) monkeys in M1. vGluT2-positive terminals form asymmetric synapses with dendritic spines (*A*–*C* and *D*, *E*) and dendritic shafts (*C*, *E* and *F*) in control and parkinsonian monkeys. Both axo-spinous and axo-dendritic synapses form macular (*B*, *C* and *E*) and perforated (*A*, *B*, *D*–*F*) PSDs in deep and superficial cortical layers from control and parkinsonian monkeys. Abbreviations: Sp: dendritc spine; D: dendrite; PSDm: macular postsynaptic density; PSDp: perforated postsynaptic density. Scale bar in *A* (applies to *B*, *D* and *E*) and in *C* (applies to *F*) = 0.5 µm.

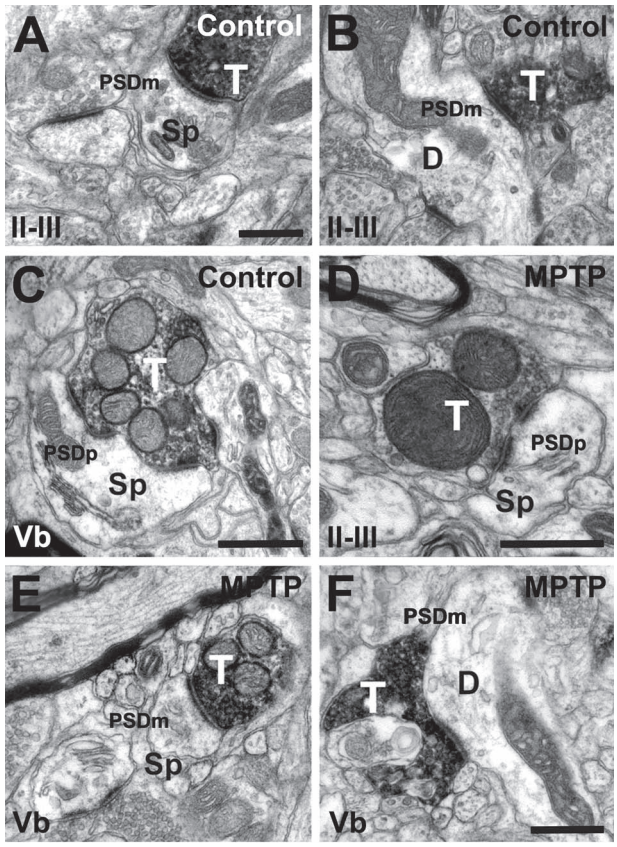

Figure 3. vGluT2-immunoreactive terminals in SMA. Immunopositive terminals in layers II–III (*A*, *B* and *D*) and layer Vb (*C*, *E* and *F*) from control (*A*–*C*) and MPTP-treated (*D*–*F*) monkeys. vGluT2-positive terminals form asymmetric synapses with dendritic spines (*A*, *C*, *D* and *E*) and dendritic shafts (*B* and *F*) in control and parkinsonian monkeys. Both axo-spinous and axo-dendritic synapses form macular (*A*, *B*, *E* and *F*) and perforated (*C*–*E*) PSDs in deep and superficial cortical layers from control and parkinsonian monkeys. Abbreviations: Sp: dendritic spine; D: dendrite; PSDm: macular postsynaptic density; PSDp: perforated post-synaptic density. Scale bar in *A* (applies to *B*), *C* (applies to *E*), *D* and *F* = 0.5 µm.

terminals, one block of tissue in layers II–III and Vb of VGluT2-immunostained cortical sections (pre-embedding immunoperoxidase method) from 6 control (3 for M1 and 3 for SMA) and 6 parkinsonian (3 for M1 and 3 for SMA) monkeys were cut in ultrathin (60-nm) sections and examined in the electron microscope. At the electron microscope level (×60 000 magnification), vGluT2-positive terminals were identified by the presence of the amorphous electron-dense peroxidase deposit (Figs 2 and 3). The vGluT2 labeling was expressed primarily on the external surface of synaptic vesicles (Hisano et al. 2000; Fremeau et al. 2001; Varoqui et al. 2002), and the ultrastructural features of these boutons were consistent with those described in previous studies from our group and others (Lacey et al. 2005; Raju et al. 2006, 2008; Kubota et al. 2007; Villalba and Smith 2010, 2011; Deng et al. 2013; Villalba and Smith 2013, 2018; Bopp et al. 2017; Zheng et al. 2019). In both layer II–III and Vb of M1 and SMA, vGluT2-positive terminals formed asymmetric synapses with either dendritic spines (Figs 2*A*–*E* and 3*A*,*C*–*E*) or dendritic shafts (Figs 2*C*,*E*,*F* and 3*B*,*F*) in control (Figs 2*A*–*C* and 3*A*–*C*) and MPTP-treated (Figs 2*D*–*F* and 3*E*,*F*) monkeys. To avoid bias, the investigator who collected electron micrographs was blinded to the health status of the animal (control vs. parkinsonian).

Quantitative Analysis of the Synaptic Connections of vGluT2-Containing Terminals

For quantitative analysis, 55–60 images of randomly encountered vGluT2-positive terminals per cortical area and layer (110–120 images per animal) were taken from the most superficial sections of the blocks to ensure optimal vGluT2 antibody penetration. For each vGluT2-positive axon terminal identified, the postsynaptic target (spine or dendritic shaft) and the PSD morphology (macular or perforated) have been quantified in superficial (II–III) and deep (Vb) layers of M1 (Figs 2, 4*A*,*C* and 5*A*; Supplementary Table 3) and SMA (Figs 3, 4*B*,*C* and 5*B*; Supplementary Table 3) in control and MPTP-treated parkinsonian monkeys. One-way ANOVAs analysis did not reveal any significant interindividual differences between the three animals in each group (M1 and SMA, control, and MPTP).

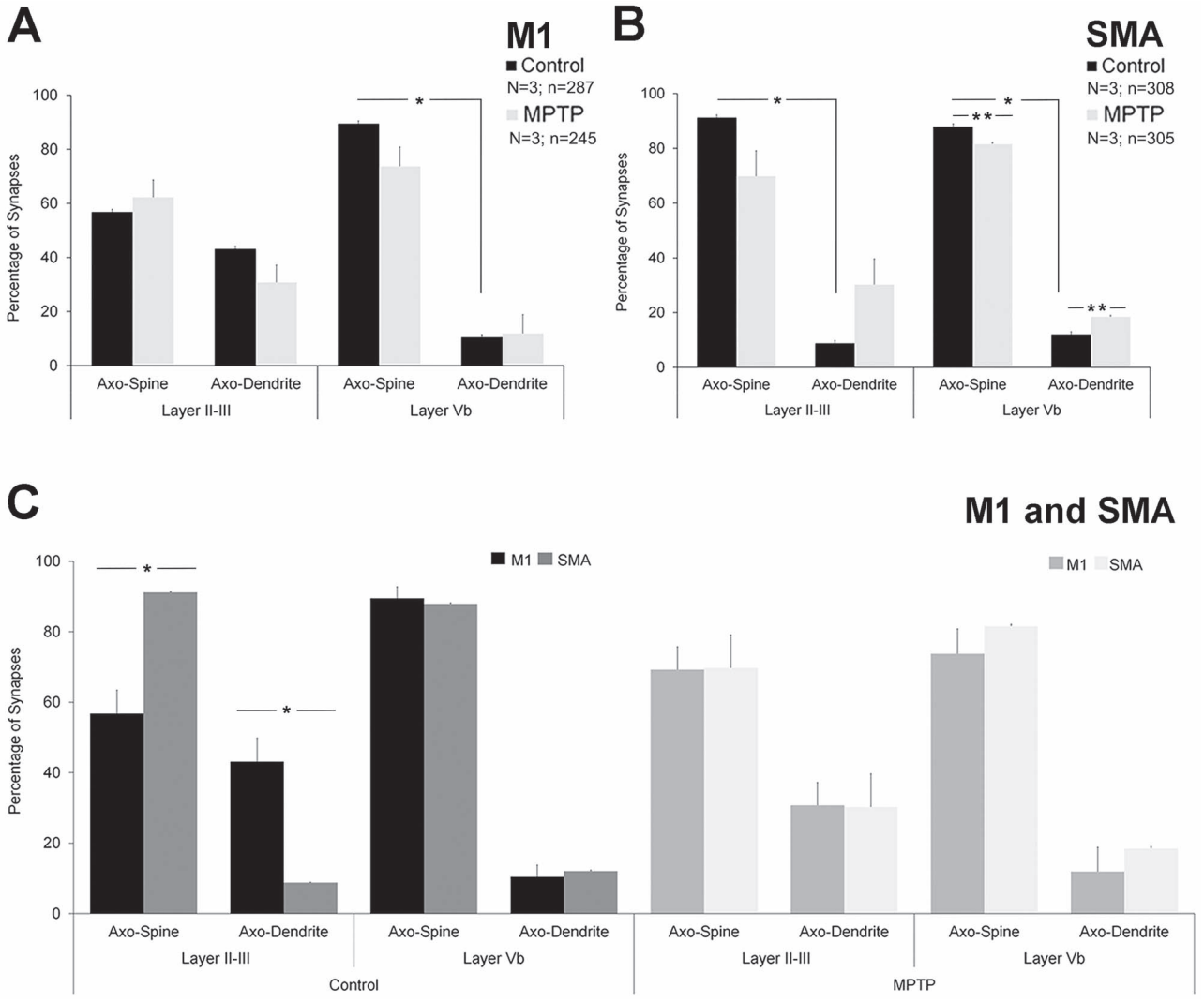

Figure 4. Comparative quantitative analysis of axo-dendritic and axo-spinous synapses formed by vGluT2-immunopositive terminals in M1 and SMA of control and parkinsonian monkeys. (*A*) In layer II–III of M1 in control monkeys, there is no significant difference in the proportion of vGluT2-positive terminals forming axo-spinous (~55–65%) versus axo-dendritic (~35–45%) synapses (Student's *t*-test, $P = 0.222$), while ~90% of vGluT2-containing terminals form axo-spinous synapses in layer Vb (axo-spinous vs. axo-dendritic; Student's *t*-test, $^{*}P \leq 0.001$). No significant differences were found between control and parkinsonian monkeys. (*B*) In the SMA of control monkeys, the percentage of vGluT2-positive terminals forming axo-spinous synapses in both layer II–III and Vb was ~10 times larger than the percentages of axo-dendritic synapses (Student's *t*-test, layer II–III and Vb $^{*}P \leq 0.001$). Significant changes in the percentages of axo-spinous and axo-dendritic synapses in layer Vb were found in parkinsonian animals (Student's *t*-test, control vs. MPTP: SMA layer II–III: axo-spinous $P = 0.085$; axo-dendritic $P = 0.085$; SMA layer Vb: axo-spinous $^{**}P \leq 0.001$; axo-dendritic $^{**}P \leq 0.001$). (*C*) Comparative analysis between M1 and SMA. Statistically significant differences in the pattern of synaptic connectivity (axo-spinous and axo-dendritic synapses) of vGluT2-containing terminals were found in layer II–III of control monkeys (Student's *t*-test, M1 vs. SMA: control: layer II–III: axo-spinous $^{*}P = 0.007$; axo-dendritic $^{*}P = 0.007$), but not in parkinsonian animals. In layer Vb, no differences were found between M1 and SMA of both control and parkinsonian monkeys. N = Number of animals; n = number of terminals analyzed.

Primary Motor Cortex

The postsynaptic targets of a total of 532 vGluT2-positive axon terminals were identified in M1 of control ($n = 287$) and parkinsonian monkeys ($n = 245$). Of these terminals, 265 were in layer II–III (144 in control; 121 in parkinsonian monkeys), while 267 were found in layer Vb (143 in control, 124 in parkinsonian monkeys) (Fig. 2 and Supplementary Table 3). In control monkeys, 56.81 ± 6.67% terminals formed synapses with dendritic spines and 43.19 ± 6.67% targeted dendritic shafts in layer II–III, while 89.51 ± 3.28% terminals terminated on spines and 10.48 ± 3.28% ended on dendritic shafts in layer Vb (Figs 2, 4A and Supplementary Table 4). There was no significant difference between the percentage of axo-dendritic and axo-spinous synapses in layer II–III (Student's *t*-test, $P = 0.222$), but axo-spinous synapses were significantly more common than axo-dendritic synapses in layer Vb (Student's *t*-test, $^{*}P \leq 0.001$) (Fig. 4A). When compared with parkinsonian monkeys, no significant differences in the relative percentages of axo-spinous and axo-dendritic synapses were found in either cortical layer (Student's *t*-test, control vs. MPTP: M1 layer II–III: axo-spinous $P = 0.252$; axo-dendritic $P = 0.252$; M1 layer Vb: axo-spinous $P = 0.114$; axo-dendritic $P = 0.104$).

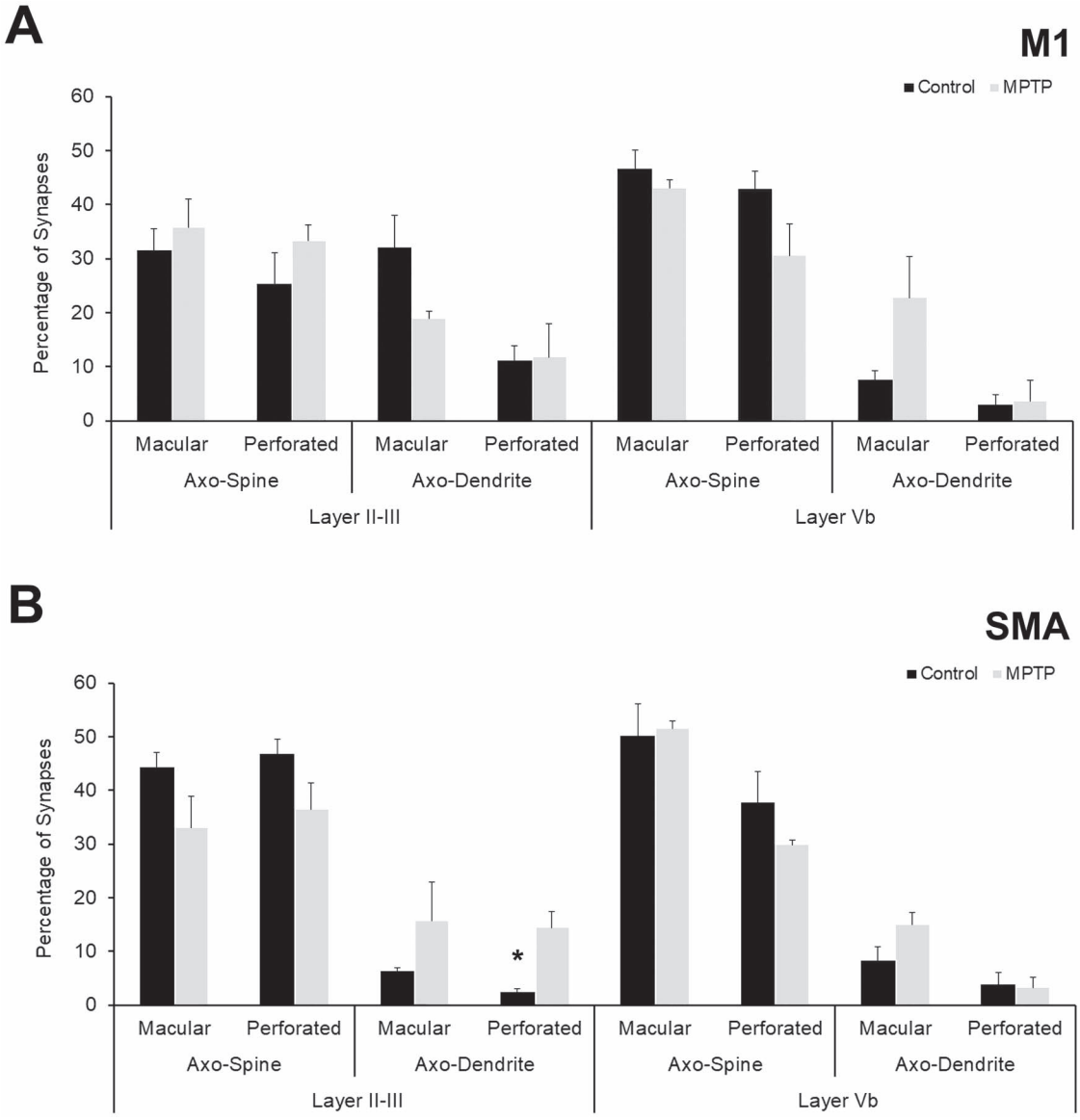

Figure 5. Quantitative analysis of PSDs (perforated vs. macular) of synapses formed by vGluT2-immunopositive synapses in superficial and deep layers in control and parkinsonian animals. (*A*) Percentage of axo-dendritic and axo-spine synapses with macular or perforated PSDs in cortical layers of M1. (*B*) Analysis of macular and perforated PSDs in cortical layers of SMA. Except for perforated axo-dendritic synapses in layer II–III of SMA (*B*), more frequently encountered in MPTP-treated monkeys than in controls (Student's *t*-test, $^{*}P = 0.007$), there are not statistically significant differences in the percentage of macular versus perforated PSDs between control and parkinsonian monkeys in both M1 (*A*) and SMA (*B*).

Supplementary Motor Area

In the SMA, the postsynaptic targets of 613 vGluT2-positive axon terminals were identified in control ($n = 308$) and parkinsonian monkeys ($n = 305$). A total of 315 of these terminals were found in layer II–III (159 in control; 156 in parkinsonian monkeys), while 298 were located in layer Vb (149 in control, 149 in parkinsonian monkeys) (Fig. 3 and Supplementary Table 3). In control monkeys, $91 \pm 0.15\%$ terminals targeted dendritic spines and $8.80 \pm 0.15\%$ formed synapses with dendritic shafts in layer II–III, while $87.93 \pm 0.3\%$ terminals terminated on spines and $12.07 \pm 0.3\%$ ended on dendritic shafts in layer Vb (Figs 3, 4*B* and Supplementary Table 3). In both layer II–III and Vb of SMA of control animals, the percentage of vGluT2-positive terminals forming axo-spinous synapses was significantly higher than those in contact with dendritic shafts (Student's *t*-test, layer II–III and Vb $^{*}P \leq 0.001$) (Fig. 4*B*). In parkinsonian monkeys, both layer II/III and layer Vb contained a larger percentage of axo-dendritic synapses than in controls, but this difference reached significance only in layer Vb (Fig. 4*B*) (Student's *t*-test, control vs. MPTP: SMA layer II–III: axo-spinous $P = 0.085$; axo-dendritic $P = 0.085$; SMA layer Vb: axo-spinous $^{**}P \leq 0.001$; axo-dendritic $^{**}P \leq 0.001$).

Primary Motor Cortex versus Supplementary Motor Area

Our comparative analysis revealed statistically significant differences (Student's *t*-test) in the relative percentages of axo-spinous and axo-dendritic synapses formed by vGluT2-positive terminals in layer II–III between M1 and SMA of control monkeys, but not in parkinsonian animals (Fig. 4*C*). In layer

Vb, no differences in the synaptic connections of vGluT2-containing terminals were found between M1 and SMA of both control and parkinsonian monkeys (Fig. 4C) (Student's *t*-test, M1 vs. SMA: control: layer II–III: axo-spinous $^{*}P = 0.007$; axo-dendritic $^{*}P = 0.007$; layer Vb: axo-spinous $P = 0.656$; axo-dendritic $P = 0.656$. MPTP: layer II–III: axo-spinous $P = 0.968$; axo-dendritic $P = 0.967$; layer Vb: axo-spinous $P = 0.335$; axo-dendritic $P = 0.309$).

Postsynaptic Densities (PSDs): Macular versus Perforated

Taking into consideration evidence that perforated PSDs are commonly associated with plasticity and increased strength of glutamatergic synapses in various brain regions (Geinisman 1993; Lisman and Harris 1993; Neuhoff et al. 1999; Geinisman 2000; Luscher et al. 2000; Sorra and Harris 2000; Harris et al. 2003; Bourne and Harris 2008; Lisman 2017; Borczyk et al. 2019; Harris 2020), we quantified the prevalence of perforated versus macular PSDs of axo-spinous and axo-dendritic synapses formed by vGluT2-positive terminals in deep and superficial layers of M1 and SMA in control and parkinsonian monkeys (Fig. 5; Supplementary Tables 3 and 4). The total number of synapses examined in this experiment was the same as the number of vGluT2-containing terminals mentioned in the previous results sections (Supplementary Table 3). In MPTP-treated monkeys, minor changes (not statistically significant) in the percentage of macular versus perforated PSDs at both axo-spinous and axo-dendritic synapses were found in M1 and SMA. Overall, there was no significant difference in the proportion of perforated and macular asymmetric PSDs associated with vGluT2-positive synapses between control and parkinsonian monkeys in both cortical layers, except for perforated axo-dendritic synapses in layer II–III of SMA, which were more frequently encountered in MPTP-treated monkeys than in controls (Student's *t*-test, $^{*}P = 0.007$).

Discussion

The results of this study provide the first comparative analysis of the pattern of synaptic organization of thalamocortical afferents in the M1 and SMA of nonhuman primates between the control and parkinsonian state. The following conclusions can be drawn: 1) There is a significant reduction in the intensity of vGluT2 immunostaining in layer Vb, but not layer II–III, of M1 and SMA of MPTP-treated parkinsonian monkeys (Fig. 6). 2) The pattern of synaptic connectivity of thalamic terminals in layers II–III, but not layer Vb, of M1 and SMA is significantly different in control monkeys. While ~90% thalamic terminals contact dendritic spines in superficial and deep layers of SMA and in layer Vb of M1, almost half vGluT2-positive thalamic terminals contact dendritic shafts in layer II–III of M1. This difference is abolished in parkinsonian animals. The higher prevalence of axo-dendritic synapses in layer II–III of M1 compared to SMA in control, but not in parkinsonian monkeys, suggests a differential thalamic drive of GABAergic interneurons between the two cortical areas in the normal state, but not in parkinsonism. 3) There is no major difference in the proportion of perforated versus macular asymmetric PSDs associated thalamic synapses between control and parkinsonian monkeys in both cortical regions. In the following account, these observations will be discussed in light of current knowledge of the anatomo-functional organization of the thalamocortical system in normal and parkinsonian states.

Thalamocortical Innervation of M1 and SMA in Control and MPTP-Treated Parkinsonian Monkeys

M1 and SMA mediate different aspects of motor control (Alexander and Crutcher 1990; Shima et al. 1991; Matsuzaka et al. 1992; Kurata 1993; Rizzolatti et al. 1996; Graziano et al. 1997; Dum and Strick 2002). While SMA is predominantly involved in the preparation and generation of sequential movements (Roland et al. 1980; Tanji and Shima 1994; Gerloff et al. 1997; Nakamura et al. 1998; Shima and Tanji 1998; Nakamura et al. 1999; Picard and Strick 2001; Hikosaka et al. 2002; Dayan and Cohen 2011), M1 is mainly responsible to produce the patterns of muscle activity that are necessary to implement the motor plans generated by the premotor areas (Karni et al. 1995; Pellizzer et al. 1995; Carpenter et al. 1999; Dayan and Cohen 2011).

Anterograde tracing studies of thalamocortical projections from different motor thalamic nuclei in monkeys have revealed that basal ganglia– and cerebellar-receiving regions of the ventral motor thalamic nuclei terminate to a variable extent in layers I, II–III, and Vb of M1 and SMA (Wiesendanger and Wiesendanger 1985; Nambu et al. 1988; Matelli et al. 1989; Darian-Smith et al. 1990; Nambu et al. 1991; Nakano et al. 1992; Darian-Smith and Darian-Smith 1993; Rouiller et al. 1994; Stepniewska et al. 1994; Inase and Tanji 1995; Shindo et al. 1995; Inase et al. 1996; Matelli and Luppino 1996; Hoover and Strick 1999; Rouiller et al. 1999; McFarland and Haber 2002; Kultas-Ilinsky et al. 2003; Morel et al. 2005; Fang et al. 2006; Stepniewska et al. 2007). Although significant knowledge has been gained about the regional pattern of thalamic inputs to motor cortex in rodents and primates using a wide range of tract-tracing methods, such is not the case for the microcircuitry of the motor thalamocortical systems, particularly in primates. In mice, progress has been made in deciphering the synaptic connectivity of M1 pyramidal neurons using electrophysiology and optogenetic methods in various strains of neuron-specific Cre transgenic mice (Lo and Anderson 2011; Kiritani et al. 2012; Tanaka et al. 2012; Hooks et al. 2013; Kaneko 2013; Hunnicutt et al. 2014; Yamawaki et al. 2014; Harris and Shepherd 2015; Yamawaki and Shepherd 2015; Bopp et al. 2017; Rodriguez-Moreno et al. 2020). Of particular relevance for the present study, Shepherd and colleagues showed that pyramidal-tract and intratelencephalic corticofugal neurons in layer II–III and Vb of M1 receive direct thalamic inputs from VA/VL, while layer VI corticothalamic neurons are almost devoid of such afferents (Hooks et al. 2013). At the electron microscopic level, only a few studies looked at the postsynaptic targets of thalamic terminals in the mouse M1. Bopp et al. (2017) showed that vGluT2-immunoreactive thalamic terminals target exclusively dendritic spines in layer IV of M1.

Along the same line, a recent study indicated that almost 95% of terminals from the posterior nucleus (PO) form axo-spinous synapses in the mouse M1 (Rodriguez-Moreno et al. 2020). Although our findings partly corroborate these observations, such that dendritic spines were the main recipients of vGluT2-containing terminals in layer II–III and Vb of SMA, we found that ~40% of vGluT2-positive terminals target dendritic shafts in layer II–III of M1 in control monkeys. Because the chemical and hodological phenotype of the thalamic-recipient cortical neurons was not characterized in our study, the functional significance of this strong dendritic innervation remains speculative. Assuming that the majority of axo-dendritic asymmetric synapses in layer II–III of M1 involves smooth dendrites of GABAergic interneurons, as commonly reported across cortices (Colonnier 1981; DeFelipe and Farinas 1992), our data suggest

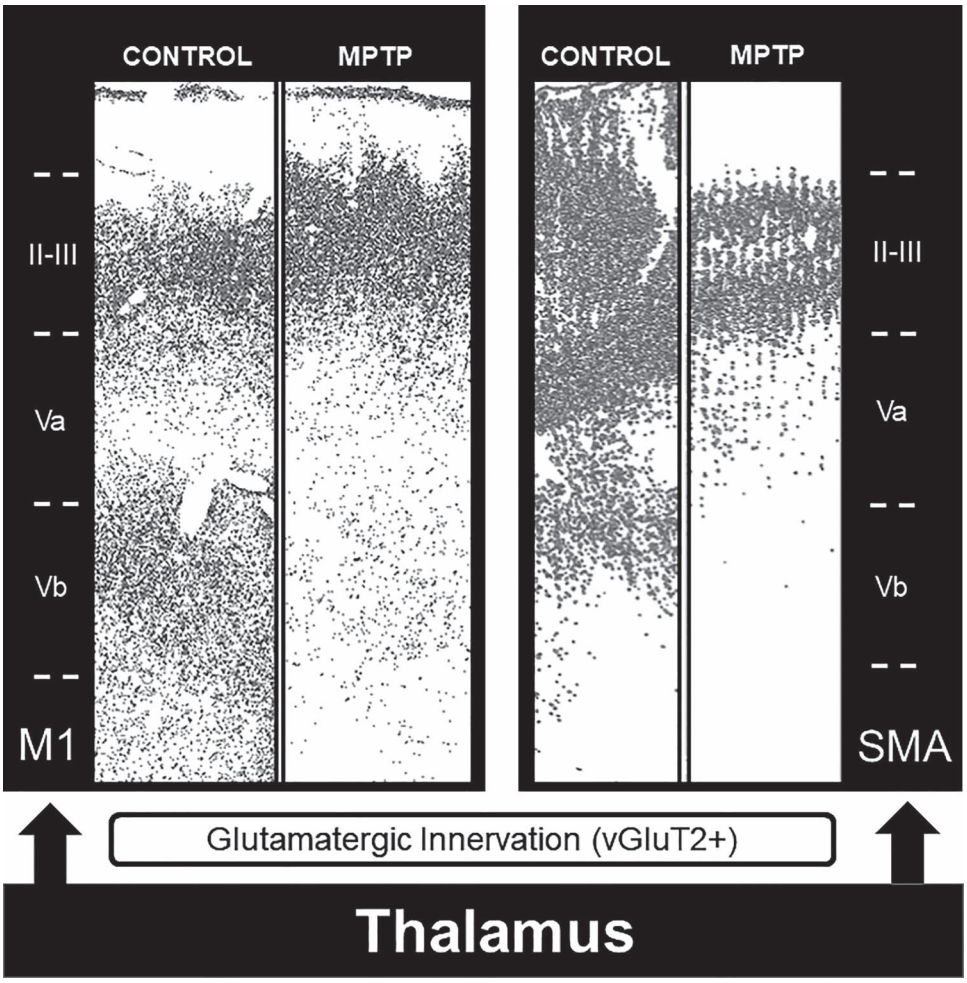

Figure 6. Summary diagram showing the vGluT2-immunostaining depletion in the deep cortical layer (Vb) of M1 and SMA in MPTP-treated parkinsonian monkeys.

that thalamic inputs may be a significant source of activation of GABAergic interneurons in superficial layers of M1. Alternatively, these findings may be indicative of an increased thalamic innervation of dendritic shafts of pyramidal neurons in this region, but this remains unlikely based on the large amount of literature showing that dendrites of pyramidal neurons in various cortical regions are almost devoid of asymmetric glutamatergic synapses (Colonnier 1981; DeFelipe and Farinas 1992). Another factor that could account for this difference may the sampled region of M1 studied in the electron microscope. In both mice studies, the areas under analysis included either layer IV only (Bopp et al. 2017), or layer IV and lower layer III (Rodriguez–Moreno et al. 2020). Although we did not attempt at delineating layer IV of M1 in our study, it is clear that the extent of vGluT2 labeling depicted in Figure 1 extends beyond the confines of the very thin layer IV that has been described in the monkey M1 (Garcia-Cabezas and Barbas 2014), suggesting that our data were mainly collected from layer III and lower layer II where the bulk of vGluT2 terminal profiles were located. In this regard, it is noteworthy that layer II–III of the neocortex underwent a significant size increase in evolution, accounting for as much as 50% of the total thickness of motor cortices in primates and only 20–25% in rodents (Hutsler et al. 2005). Whether this dramatic expansion of layer II–III is associated with a differential pattern of thalamic innervation of interneurons versus projection neurons remains to be established. Another important consideration is the fact that the percentage of neocortical GABAergic interneurons is significantly larger in primates than rodents and that most of these interneurons lay within layer I–III of M1 in monkeys (Hendry et al. 1987; Sherwood et al. 2010; Young et al. 2013).

In MPTP-treated parkinsonian monkeys, this differential dendritic innervation of layer II–III between M1 and SMA was abolished, such that ~30% of vGluT2-positive terminals formed axo-dendritic asymmetric synapses in both cortical regions. This change is largely due to an increased percentage of axo-dendritic over axo-spinous thalamocortical synapses in layer II–III of SMA in parkinsonian monkeys. A potential source of the increased ratio of axo-dendritic/axo-spinous synapses formed by thalamocortical terminals in the SMA of parkinsonian monkeys could be a reduced density of dendritic spines on subsets of SMA corticofugal neurons. Although spine pruning and plasticity has not been addressed in detail in the cortex of animal models of parkinsonism and PD patients, spine loss is a key pathological feature of striatal projection neurons in PD (Ingham et al. 1989; Stephens et al. 2005; Zaja-Milatovic et al. 2005; Smith et al. 2009; Villalba et al. 2009; Villalba and Smith 2010, 2013, 2018; Smith et al. 2012). At the cortical level, spine loss has been reported in the dorsolateral prefrontal cortex and M1 of MPTP-treated monkeys, while other cortical regions, like the cingulate and enthorhinal cortices, did not exhibit signicant

spine pathology, suggesting that this pathology affects specific cortical regions (Smith et al. 2013; Elsworth et al. 2013). Further detailed quantitative assessment of spine loss in different subsets of projection neurons in M1 and SMA of parkinsonian monkeys are needed to directly address this issue.

In rodents, there is evidence that many spines targeted by vGluT2-containing terminals in the motor cortex also receive innervation from unlabeled terminals forming symmetric synapses (Kubota et al. 2007). Although such convergence was rarely seen in our material, we cannot rule out that this may be an underestimate because our observations were collected from single ultrathin sections. Three-dimensional EM reconstruction of individual spines and their synaptic afferents is needed to directly address this issue.

Pathophysiology of Specific Subtypes of Corticofugal Neurons in Parkinsonism

Electrophysiological studies in nonhuman primates have shown that specific populations of corticofugal neurons are differentially affected by parkinsonism. In M1, prior to MPTP administration, corticostriatal neurons have spontaneous firing rates markedly lower than pyramidal tract projection neurons (Bauswein et al. 1989; Turner and DeLong 2000). In MPTP-treated parkinsonian monkeys, pyramidal tract projection neurons, but not corticostriatal cells, become more bursty and less likely to fire in a regular-spiking pattern and show an increased propensity for rhythmic spiking in the beta frequency range (14–32 Hz) (Pasquereau and Turner 2011, 2013). Given that pyramidal tract corticofugal neurons are the primary sources of motor commands to the spinal cord, their dysfunction is likely to contribute to the pathophysiology of parkinsonian motor signs (Pasquereau and Turner 2011, 2013). Although the exact contibuting factors to these activity changes remain to be established, disruption of the cortical synaptic microcircuitry of both pyramidal projection neurons and GABAergic interneurons should be considered. As indicated by our findings and others, the dendrites of GABAergic interneurons are targeted by thalamocortical afferents in various cortical regions (Hendry and Jones 1983; Kultas-Ilinsky et al. 1985; Gabernet et al. 2005; Bragina et al. 2007; Brecht et al. 2013; Luo et al. 2019). These findings, combined with evidence that reduced M1 interneurons activity may contribute to the development of irregular and rhythmic firing of pyramidal neurons in the beta frequency (Lefaucheur 2005; Brazhnik et al. 2012), further highlights the importance of thalamic regulation of both projection neurons and interneurons in the development of cortical pathophysiology in the parkinsonian state. Future studies of specific subtypes of thalamic-recipient pyramidal neurons in M1 and SMA affected morphologically and functionally by changes in thalamocortical connectivity in parkinsonian animals are needed to further understand the synaptic networks and mechanisms through which thalamic afferents regulate or dysregulate motor cortical activity in normal and parkinsonian conditions.

Does Thalamic Pathology in Caudal Intralaminar Nuclei Account for the Layer-Specific Loss of vGluT2 Neuropil Immunoreactivity in M1 and SMA?

Our data showed a significant decrease of vGluT2 immunoreactivity in layer Vb of both M1 and SMA in parkinsonian monkeys. Although the exact source of this reduced vGluT2 innervation remains to be established, one possibility is the potential deafferentation of layer V from its caudal intralaminar thalamic innervation. In addition to the ventral motor thalamus, the caudal intralaminar thalamic nuclei, specifically the CM nucleus, indeed, project to layer V of M1 with minimal projections to upper layers (Parent and Parent 2005). In light of data showing a loss of CM/Pf neurons in MPTP-treated parkinsonian monkeys (Villalba, Wichmann, et al. 2014a; Villalba et al. 2019), 6-OHDA-treated rats (Aymerich et al. 2006) and PD patients (Henderson et al. 2000a, 2000b), one may speculate that the neuronal degeneration in CM underlies some of the drastic loss of thalamic inputs to deep cortical layers of M1 and SMA described in the present study. Interestingly, the loss of vGluT2 immunostaining was not associated with a change in the relative ratio of axo-dendritic versus axo-spinous synapses formed by vGluT2-positive terminals in layer Vb of either cortical regions, such that in both control and parkinsonian monkeys, ~90% of vGluT2-immunoreactive terminals contacted dendritic spines, while the remaining terminals formed axo-dendritic synapses. However, it is important to note that our electron microscopy analysis does not provide information about the changes in the total number of vGluT2-containing terminals between control and parkinsonian animals. We cannot rule out we cannot rule out the possibility that the decrease in vGluT2 immunoreactivity in layer Vb of parkinsonian monkeys may be related to a reduced expression of vGluT2 protein in thalamic terminals, instead of thalamocortical terminal loss. Unbiased stereological terminal counts of vGluT2-immunoreactive terminal profiles in specific layers of M1 and SMA in control and parkinsonian monkeys is in progress to directly address this issue. In contrast to this decreased thalamic innervation, we did not find any significant difference in the vGluT1-containing cortico-cortical connections of M1 and SMA between control and parkinsonian monkeys (Villalba et al. 2018), suggesting the specificity of this pathology for the thalamocortical system. Future optogenetic studies that compare the impact of CM-cortical activation on the firing of layer V pyramidal cells between control and parkinsonian monkeys are needed to assess the functional significance of these anatomical changes.

In addition to layer Vb and II–III, layer I also receives a significant vGluT2-containing thalamic innervation, some of which originating from the ventral motor thalamic nuclei (McFarland and Haber 2002). As described in the visual cortex, the vGluT2 innervation of layer I of M1 and SMA may be supplied by axon collaterals of thalamic inputs to layer II–III (Garcia-Marin et al. 2013). In the present study, we did not compare the density of vGluT2 innervation of layer I between control and parkinsonian monkeys because of the variable quality of brain tissue in this layer due to its uneven thickness in vibratome sections. A detailed analysis of vGluT2 labeling in layer I must be achieved using frozen sections that better preserve the integrity of this superficial lamina.

Morphology of Postsynaptic Densities (PSDs) of Thalamocortical Synapses in M1 and SMA of Parkinsonian Monkeys

The presence of segmented or completely partitioned PSDs (perforated PSDs) has been considered a structural modification associated with increased synaptic efficacy and learning (Nieto-Sampedro et al. 1982; Lisman and Harris 1993). The compartmentalization of multiple transmission zones impedes the saturation of postsynaptic receptors and allows multiple

transmitter quanta to be effective at the same postsynaptic spine, thereby enhancing the strength of individual synapses (Lisman and Harris 1993; Bell et al. 2014; Chirillo et al. 2019; Harris 2020). In the striatum of human parkinsonian and animal models of PD, an increased prevalence of perforated PSDs at glutamatergic axo-spinous synapses has been linked with an increased strength of corticostriatal synapses (Anglade et al. 1996; Ingham et al. 1998; Meshul et al. 1999, 2000; Villalba and Smith 2010, 2011, 2013; Villalba et al. 2015). Our ultrastructural analysis did not reveal any significant difference in the relative prevalence of macular versus perforated glutamatergic thalamostriatal synapses in M1 and SMA of parkinsonian monkeys, except for an increased percentage of perforated axo-dendritic synapses in layer II–III of SMA. Although the functional significance of this structural change remains to be determined, one could speculate that it may be linked with an increased drive or changes in synaptic properties of thalamic inputs to GABAergic interneurons. Future optogenetic studies are needed to directly address this issue.

It is noteworthy that ultrathin sections were not collected serially in the present study, thereby restricting the analysis of PSDs morphology to be achieved from single 2D images. This approach may have underestimated the absolute number of perforated synapses. However, because the same single-section analysis was used to examine the relative prevalence of either synapse subtypes in control and parkinsonian monkeys, this technical limitation does not hamper conclusions made from these data. Ongoing 3D EM studies using serial images from each cortical layer are in progress in our laboratory to further study the morphometry and absolute abundance of macular versus perforated PSDs in each cortical layer in an established 3D volume.

Technical Considerations

Due to limited availability of nonhuman primates to be used in our study, the age of animals in the different groups is variable ranging from 1 years, 9 months to 17 years, 5 months (Table 1), which may raise concerns about the impact such an age difference may have on the conclusions made in the present study. This issue is particularly critical for the SMA because the three animals in the control groups are younger than the animals used in the MPTP group (Table 1). Although, we cannot rule out that this difference in age may contribute to some differences in vGluT2 densitometry measurements, various data from our study and previous literature suggest otherwise. First, an extensive study of the developmental regulation of the density of symmetric and asymmetric synapses in various layers of M1 (Zecevic et al. 1989) indicated that the density of asymmetric synapses in layers II–III and V of M1 of rhesus monkeys reach a peak at about 2 months old and then slowly decrease toward the adult values until sexual maturity (3 years old). Although such a detailed analysis is not available for SMA and does not focus specifically on the development of vGluT2 thalamocortical innervation, it remains a valuable data set to interpret our results. Although two of the monkeys used in the SMA control group (MR249, MR256) had not yet reached sexual maturity at the time of euthanasia, the animal MR252 was 3 years 9 months, thus sexually mature. As shown in Supplementary Table 2, the difference in age between MR249 (1 years 9 months) and MR252 (3 years 9 months) had no significant influence on the densitometry measurement values collected from layer Vb in these two control monkeys. On average, the layer Vb densitometry values for MR252 and MR249 were 35 and 39, respectively. In regard to layer II–III, the average measurements were slightly larger in MR249 (170) than in MR252 (136), but these values were in the same ball park as measurements taken from layer II–III in M1 of MR194 (13 years 2 months; 137) and MR212 (10 years 8 months; 166). Based on these observations, we consider that the variability in age of animals used in this study is unlikely to account for the differences in vGluT2 immunoreactivity densitometry measurements between control and parkinsonian monkeys.

Similarly, it is unlikely that age differences could explain the variations in synaptic connections and PSDs morphology of vGluT2-positive terminals described in our study. For instance, the ratio of macular/perforated axo-dendritic asymmetric synapses between the youngest (MR241, 1 years, 9 months) and oldest (MR252, 3 years, 9 months) animal of the control SMA group is within the same range, suggesting that the young age of MR241 did not significantly shift the control values in a direction strikingly different from those gathered in adult monkeys. It is also noteworthy that the ratios between the two types of synapses found in control monkeys are close to those found for two of the 6 years old MPTP-treated monkeys (Supplementary Table 2). These observations, combined with data from the literature indicating that the relative prevalence of complex perforated axo-spinous and axo-dendritic asymmetric synapses increase with age in M1 (Zecevic et al. 1989) argue against the fact that the young age of control SMA monkeys is the main source of findings shown in Figure 5B.

Finally, there are two arguments against the idea that age difference may be the main contributor of differences seen in the relative proportion of axo-spinous versus axo-dendritic synapses between M1 and SMA (Fig. 4C). First, values from each animal in either M1 or SMA are comparable despite the age difference of the animals (see Supplementary Table 2). Second, evidence from the literature indicates that the ratio of axo-dendritic versus axo-spinous asymmetric synapses increases with age in M1 (Zecevic et al. 1989). Assuming that such is the case as well for SMA, it is unlikely that the young age of control monkeys used for SMA studies explains the increased prevalence of axo-dendritic synapses in layer II–III of SMA versus M1 reported in Figure 4C.

Concluding Remarks

Although much remains to be known about the pathophysiology of motor cortices in parkinsonism, our findings suggest that neuroplastic changes in the extent and pattern of synaptic connectivity of thalamocortical projections may contribute to the disruption of the motor basal ganglia-thalamocortical loop in the parkinsonian state (Fig. 6). A deeper understanding of the underlying substrate of the thalamic denervation of layer Vb in M1 and SMA of parkinsonian animals is of utmost importance. Ongoing anatomical and functional experiments aimed at determining the contribution of CM degeneration to this pathology could open up the possibility that the pathophysiology of thalamocortical systems in PD does not rely solely on the disruption of motor-related output from the ventral motor thalamus but also involve reduced attention-related influences from the caudal intralaminar complex (Matsumoto et al. 2001; Smith et al. 2011, 2014). Another important area of future investigations laid out by our anatomical observations is the possibility for a differential regulation of layer II–III GABAergic interneurons by thalamic inputs between M1 and SMA in control and parkinsonian states.

Supplementary Material

Supplementary material can be found at *Cerebral Cortex* online.

Notes

The authors thank Susan Jenkins for technical assistance. *Conflict of Interest*: All authors declare no potential conflict of interests.

Funding

This work was supported by the National Institute of Health (grant P50NS098685); the National Institute of Health/Office of Research Infrastructure Programs P51 (grant P51OD011132) of the Yerkes National Primate Research Center.

References

Albin RL, Young AB, Penney JB. 1989. The functional anatomy of basal ganglia disorders. *Trends Neurosci*. 12:366–375.

Alexander GE, Crutcher MD. 1990. Neural representations of the target (goal) of visually guided arm movements in three motor areas of the monkey. *J Neurophysiol*. 64:164–178.

Altar CA, Heikkila RE, Manzino L, Marien MR. 1986. 1-Methyl-4-phenylpyridine (MPP+): regional dopamine neuron uptake, toxicity, and novel rotational behavior following dopamine receptor proliferation. *Eur J Pharmacol*. 131:199–209.

Amitai Y. 2001. Thalamocortical synaptic connections: efficacy, modulation, inhibition and plasticity. *Rev Neurosci*. 12:159–173.

Anglade P, Mouatt-Prigent A, Agid Y, Hirsch E. 1996. Synaptic plasticity in the caudate nucleus of patients with Parkinson's disease. *Neurodegeneration*. 5:121–128.

Arbuthnott GW, MacLeod NK, Maxwell DJ, Wright AK. 1990. Distribution and synaptic contacts of the cortical terminals arising from neurons in the rat ventromedial thalamic nucleus. *Neuroscience*. 38:47–60.

Aumann TD, Ivanusic J, Horne MK. 1998. Arborisation and termination of single motor thalamocortical axons in the rat. *J Comp Neurol*. 396:121–130.

Aymerich MS, Barroso-Chinea P, Perez-Manso M, Munoz-Patino AM, Moreno-Igoa M, Gonzalez-Hernandez T, Lanciego JL. 2006. Consequences of unilateral nigrostriatal denervation on the thalamostriatal pathway in rats. *Eur J Neurosci*. 23:2099–2108.

Bauswein E, Fromm C, Preuss A. 1989. Corticostriatal cells in comparison with pyramidal tract neurons: contrasting properties in the behaving monkey. *Brain Res*. 493:198–203.

Behnke JA, Villalba RM, Pare JF, Jenkins S, Smith Y. 2017. Reorganization of thalamocortical glutamatergic synapses in the supplementary motor area (SMA) of MPTP-treated parkinsonian monkeys. *Soc Neurosci Abstr*. Program No 757.08. On line.

Bell ME, Bourne JN, Chirillo MA, Mendenhall JM, Kuwajima M, Harris KM. 2014. Dynamics of nascent and active zone ultrastructure as synapses enlarge during long-term potentiation in mature hippocampus. *J Comp Neurol*. 522:3861–3884.

Bopp R, Holler-Rickauer S, Martin KA, Schuhknecht GF. 2017. An ultrastructural study of the thalamic input to layer 4 of primary motor and primary somatosensory cortex in the mouse. *J Neurosci*. 37:2435–2448.

Borczyk M, Sliwinska MA, Caly A, Bernas T, Radwanska K. 2019. Neuronal plasticity affects correlation between the size of dendritic spine and its postsynaptic density. *Sci Rep*. 9:1693.

Bourne JN, Harris KM. 2008. Balancing structure and function at hippocampal dendritic spines. *Annu Rev Neurosci*. 31:47–67.

Bragina L, Candiracci C, Barbaresi P, Giovedi S, Benfenati F, Conti F. 2007. Heterogeneity of glutamatergic and GABAergic release machinery in cerebral cortex. *Neuroscience*. 146:1829–1840.

Brazhnik E, Cruz AV, Avila I, Wahba MI, Novikov N, Ilieva NM, McCoy AJ, Gerber C, Walters JR. 2012. State-dependent spike and local field synchronization between motor cortex and substantia nigra in hemiparkinsonian rats. *J Neurosci*. 32:7869–7880.

Brecht M, Hatsopoulos NG, Kaneko T, Shepherd GM. 2013. Motor cortex microcircuits. *Front Neural Circuits*. 7:196.

Brown AR, Hu B, Antle MC, Teskey GC. 2009. Neocortical movement representations are reduced and reorganized following bilateral intrastriatal 6-hydroxydopamine infusion and dopamine type-2 receptor antagonism. *Exp Neurol*. 220:162–170.

Carpenter AF, Georgopoulos AP, Pellizzer G. 1999. Motor cortical encoding of serial order in a context-recall task. *Science*. 283:1752–1757.

Castro-Alamancos MA, Connors BW. 1997. Thalamocortical synapses. *Prog Neurobiol*. 51:581–586.

Chirillo MA, Waters MS, Lindsey LF, Bourne JN, Harris KM. 2019. Local resources of polyribosomes and SER promote synapse enlargement and spine clustering after long-term potentiation in adult rat hippocampus. *Sci Rep*. 9:3861.

Chu HY. 2020. Synaptic and cellular plasticity in Parkinson's disease. *Acta Pharmacol Sin*. 41:447–445.

Colonnier M. 1981. The electron-microscopic analysis of the neuronal organization of the cerebral cortex. In: Schmitt FO, Worden FG, Adelman G, Dennis SG, editors. *The organization of the cerebral cortex*. Cambridge (MA): MIT Press, pp. 125–152.

Cruikshank SJ, Lewis TJ, Connors BW. 2007. Synaptic basis for intense thalamocortical activation of feedforward inhibitory cells in neocortex. *Nat Neurosci*. 10:462–468.

Cunnington R, Egan GF, O'Sullivan JD, Hughes AJ, Bradshaw JL, Colebatch JG. 2001. Motor imagery in Parkinson's disease: a PET study. *Mov Disord*. 16:849–857.

Darian-Smith C, Darian-Smith I. 1993. Thalamic projections to areas 3a, 3b, and 4 in the sensorimotor cortex of the mature and infant macaque monkey. *J Comp Neurol*. 335: 173–199.

Darian-Smith C, Darian-Smith I, Cheema SS. 1990. Thalamic projections to sensorimotor cortex in the macaque monkey: use of multiple retrograde fluorescent tracers. *J Comp Neurol*. 299:17–46.

Day M, Wang Z, Ding J, An X, Ingham CA, Shering AF, Wokosin D, Ilijic E, Sun Z, Sampson AR, et al. 2006. Selective elimination of glutamatergic synapses on striatopallidal neurons in Parkinson disease models. *Nat Neurosci*. 9:251–259.

Dayan E, Cohen LG. 2011. Neuroplasticity subserving motor skill learning. *Neuron*. 72:443–454.

DeFelipe J, Farinas I. 1992. The pyramidal neuron of the cerebral cortex: morphological and chemical characteristics of the synaptic inputs. *Prog Neurobiol*. 39:563–607.

DeLong MR. 1990. Primate models of movement disorders of basal ganglia origin. *Trends Neurosci*. 13:281–285.

DeLong MR, Wichmann T. 2007. Circuits and circuit disorders of the basal ganglia. *Arch Neurol*. 64:20–24.

Deng YP, Wong T, Bricker-Anthony C, Deng B, Reiner A. 2013. Loss of corticostriatal and thalamostriatal synaptic terminals precedes striatal projection neuron pathology in heterozygous Q140 Huntington's disease mice. *Neurobiol Dis*. 60:89–107.

Doig NM, Moss J, Bolam JP. 2010. Cortical and thalamic innervation of direct and indirect pathway medium-sized spiny neurons in mouse striatum. *J Neurosci*. 30:14610–14618.

Doudet DJ, Gross C, Arluison M, Bioulac B. 1990. Modifications of precentral cortex discharge and EMG activity in monkeys with MPTP-induced lesions of DA nigral neurons. *Exp Brain Res*. 80:177–188.

Dum RP, Strick PL. 2002. Motor areas in the frontal lobe of the primate. *Physiol Behav*. 77:677–682.

Elsworth JD, Leranth C, Redmond DE Jr, Roth RH. 2013. Loss of asymmetric spine synapses in prefrontal cortex of motor-asymptomatic, dopamine-depleted, cognitively impaired MPTP-treated monkeys. *Int J Neuropsychopharmacol*. 16:905–912.

Escola L, Michelet T, Macia F, Guehl D, Bioulac B, Burbaud P. 2003. Disruption of information processing in the supplementary motor area of the MPTP-treated monkey: a clue to the pathophysiology of akinesia? *Brain*. 126:95–114.

Fang PC, Stepniewska I, Kaas JH. 2006. The thalamic connections of motor, premotor, and prefrontal areas of cortex in a prosimian primate (*Otolemur garnetti*). *Neuroscience*. 143:987–1020.

Fremeau RT Jr, Troyer MD, Pahner I, Nygaard GO, Tran CH, Reimer RJ, Bellocchio EE, Fortin D, Storm-Mathisen J, Edwards RH. 2001. The expression of vesicular glutamate transporters defines two classes of excitatory synapse. *Neuron*. 31:247–260.

Gabernet L, Jadhav SP, Feldman DE, Carandini M, Scanziani M. 2005. Somatosensory integration controlled by dynamic thalamocortical feed-forward inhibition. *Neuron*. 48:315–327.

Galvan A, Devergnas A, Wichmann T. 2015. Alterations in neuronal activity in basal ganglia-thalamocortical circuits in the parkinsonian state. *Front Neuroanat*. 9:5.

Garcia-Cabezas MA, Barbas H. 2014. Area 4 has layer IV in adult primates. *Eur J Neurosci*. 39:1824–1834.

Garcia-Marin V, Ahmed TH, Afzal YC, Hawken MJ. 2013. Distribution of vesicular glutamate transporter 2 (vGluT2) in the primary visual cortex of the macaque and human. *J Comp Neurol*. 521:130–151.

Geinisman Y. 1993. Perforated axospinous synapses with multiple, completely partitioned transmission zones: probable structural intermediates in synaptic plasticity. *Hippocampus*. 3:417–433.

Geinisman Y. 2000. Structural synaptic modifications associated with hippocampal LTP and behavioral learning. *Cereb Cortex*. 10:952–962.

Gerloff C, Corwell B, Chen R, Hallett M, Cohen LG. 1997. Stimulation over the human supplementary motor area interferes with the organization of future elements in complex motor sequences. *Brain*. 120:1587–1602.

Goldberg JA, Boraud T, Maraton S, Haber SN, Vaadia E, Bergman H. 2002. Enhanced synchrony among primary motor cortex neurons in the 1-methyl-4-phenyl-1,2,3,6-tetrahydropyridine primate model of Parkinson's disease. *J Neurosci*. 22:4639–4653.

Goldberg JH, Farries MA, Fee MS. 2012. Integration of cortical and pallidal inputs in the basal ganglia-recipient thalamus of singing birds. *J Neurophysiol*. 108:1403–1429.

Graziano A, Liu XB, Murray KD, Jones EG. 2008. Vesicular glutamate transporters define two sets of glutamatergic afferents to the somatosensory thalamus and two thalamocortical projections in the mouse. *J Comp Neurol*. 507:1258–1276.

Graziano MS, Hu XT, Gross CG. 1997. Visuospatial properties of ventral premotor cortex. *J Neurophysiol*. 77:2268–2292.

Halliday GM. 2009. Thalamic changes in Parkinson's disease. *Parkinsonism Relat Disord*. 15:S152–S155.

Harris KD, Shepherd GM. 2015. The neocortical circuit: themes and variations. *Nat Neurosci*. 18:170–181.

Harris KM. 2020. Synaptic odyssey. *J Neurosci*. 40:61–80.

Harris KM, Fiala JC, Ostroff L. 2003. Structural changes at dendritic spine synapses during long-term potentiation. *Philos Trans R Soc Lond B Biol Sci*. 358:745–748.

Harris KM, Weinberg RJ. 2012. Ultrastructure of synapses in the mammalian brain. *Cold Spring Harb Perspect Biol*. 4:a005587.

Haslinger B, Erhard P, Kampfe N, Boecker H, Rummeny E, Schwaiger M, Conrad B, Ceballos-Baumann AO. 2001. Event-related functional magnetic resonance imaging in Parkinson's disease before and after levodopa. *Brain*. 124:558–570.

Henderson JM, Carpenter K, Cartwright H, Halliday GM. 2000a. Degeneration of the Centre median-parafascicular complex in Parkinson's disease. *Ann Neurol*. 47:345–352.

Henderson JM, Carpenter K, Cartwright H, Halliday GM. 2000b. Loss of thalamic intralaminar nuclei in progressive supranuclear palsy and Parkinson's disease: clinical and therapeutic implications. *Brain*. 123:1410–1421.

Hendry SH, Jones EG. 1983. The organization of pyramidal and non-pyramidal cell dendrites in relation to thalamic afferent terminations in the monkey somatic sensory cortex. *J Neurocytol*. 12:277–298.

Hendry SH, Schwark HD, Jones EG, Yan J. 1987. Numbers and proportions of GABA-immunoreactive neurons in different areas of monkey cerebral cortex. *J Neurosci*. 7:1503–1519.

Herkenham M. 1980. Laminar organization of thalamic projections to the rat neocortex. *Science*. 207:532–535.

Herkenham M, Little MD, Bankiewicz K, Yang SC, Markey SP, Johannessen JN. 1991. Selective retention of MPP+ within the monoaminergic systems of the primate brain following MPTP administration: an in vivo autoradiographic study. *Neuroscience*. 40:133–158.

Herzog E, Bellenchi GC, Gras C, Bernard V, Ravassard P, Bedet C, Gasnier B, Giros B, El Mestikawy S. 2001. The existence of a second vesicular glutamate transporter specifies subpopulations of glutamatergic neurons. *J Neurosci*. 21: RC181.

Hikosaka O, Nakamura K, Sakai K, Nakahara H. 2002. Central mechanisms of motor skill learning. *Curr Opin Neurobiol*. 12:217–222.

Hisano S, Hoshi K, Ikeda Y, Maruyama D, Kanemoto M, Ichijo H, Kojima I, Takeda J, Nogami H. 2000. Regional expression of a gene encoding a neuron-specific Na(+)-dependent inorganic phosphate cotransporter (DNPI) in the rat forebrain. *Brain Res Mol Brain Res*. 83:34–43.

Hooks BM, Mao T, Gutnisky DA, Yamawaki N, Svoboda K, Shepherd GM. 2013. Organization of cortical and thalamic input to pyramidal neurons in mouse motor cortex. *J Neurosci*. 33:748–760.

Hoover JE, Strick PL. 1999. The organization of cerebellar and basal ganglia outputs to primary motor cortex as revealed by retrograde transneuronal transport of herpes simplex virus type 1. *J Neurosci*. 19:1446–1463.

Hunnicutt BJ, Long BR, Kusefoglu D, Gertz KJ, Zhong H, Mao T. 2014. A comprehensive thalamocortical projection map at the mesoscopic level. *Nat Neurosci*. 17:1276–1285.

Hutsler JJ, Lee DG, Porter KK. 2005. Comparative analysis of cortical layering and supragranular layer enlargement in rodent carnivore and primate species. *Brain Res*. 1052:71–81.

Ichikawa M, Arissian K, Asanuma H. 1985. Distribution of corticocortical and thalamocortical synapses on identified motor cortical neurons in the cat: Golgi, electron microscopic and degeneration study. *Brain Res*. 345:87–101.

Inase M, Tanji J. 1995. Thalamic distribution of projection neurons to the primary motor cortex relative to afferent terminal fields from the globus pallidus in the macaque monkey. *J Comp Neurol*. 353:415–426.

Inase M, Tokuno H, Nambu A, Akazawa T, Takada M. 1996. Origin of thalamocortical projections to the presupplementary motor area (pre-SMA) in the macaque monkey. *Neurosci Res*. 25:217–227.

Ingham CA, Hood SH, Arbuthnott GW. 1989. Spine density on neostriatal neurones changes with 6-hydroxydopamine lesions and with age. *Brain Res*. 503:334–338.

Ingham CA, Hood SH, Taggart P, Arbuthnott GW. 1998. Plasticity of synapses in the rat neostriatum after unilateral lesion of the nigrostriatal dopaminergic pathway. *J Neurosci*. 18:4732–4743.

Johannessen JN. 1991. A model of chronic neurotoxicity: long-term retention of the neurotoxin 1-methyl-4-phenylpyridinium (MPP+) within catecholaminergic neurons. *Neurotoxicology*. 12:285–302.

Kaneko T. 2013. Local connections of excitatory neurons in motor-associated cortical areas of the rat. *Front Neural Circuits*. 7:75.

Karni A, Meyer G, Jezzard P, Adams MM, Turner R, Ungerleider LG. 1995. Functional MRI evidence for adult motor cortex plasticity during motor skill learning. *Nature*. 377: 155–158.

Kashani A, Betancur C, Giros B, Hirsch E, El Mestikawy S. 2007. Altered expression of vesicular glutamate transporters vGLUT1 and vGLUT2 in Parkinson disease. *Neurobiol Aging*. 28:568–578.

Kiritani T, Wickersham IR, Seung HS, Shepherd GM. 2012. Hierarchical connectivity and connection-specific dynamics in the corticospinal-corticostriatal microcircuit in mouse motor cortex. *J Neurosci*. 32:4992–5001.

Kubota Y, Hatada S, Kondo S, Karube F, Kawaguchi Y. 2007. Neocortical inhibitory terminals innervate dendritic spines targeted by thalamocortical afferents. *J Neurosci*. 27: 1139–1150.

Kultas-Ilinsky K, Ribak CE, Peterson GM, Oertel WH. 1985. A description of the GABAergic neurons and axon terminals in the motor nuclei of the cat thalamus. *J Neurosci*. 5:1346–1369.

Kultas-Ilinsky K, Sivan-Loukianova E, Ilinsky IA. 2003. Reevaluation of the primary motor cortex connections with the thalamus in primates. *J Comp Neurol*. 457:133–158.

Kuramoto E, Furuta T, Nakamura KC, Unzai T, Hioki H, Kaneko T. 2009. Two types of thalamocortical projections from the motor thalamic nuclei of the rat: a single neuron-tracing study using viral vectors. *Cereb Cortex*. 19:2065–2077.

Kuramoto E, Ohno S, Furuta T, Unzai T, Tanaka YR, Hioki H, Kaneko T. 2015. Ventral medial nucleus neurons send thalamocortical afferents more widely and more preferentially to layer 1 than neurons of the ventral anterior-ventral lateral nuclear complex in the rat. *Cereb Cortex*. 25:221–235.

Kurata K. 1993. Premotor cortex of monkeys: set- and movement-related activity reflecting amplitude and direction of wrist movements. *J Neurophysiol*. 69:187–200.

Lacey CJ, Boyes J, Gerlach O, Chen L, Magill PJ, Bolam JP. 2005. GABA(B) receptors at glutamatergic synapses in the rat striatum. *Neuroscience*. 136:1083–1095.

Lefaucheur JP. 2005. Motor cortex dysfunction revealed by cortical excitability studies in Parkinson's disease: influence of antiparkinsonian treatment and cortical stimulation. *Clin Neurophysiol*. 116:244–253.

Lindenbach D, Bishop C. 2013. Critical involvement of the motor cortex in the pathophysiology and treatment of Parkinson's disease. *Neurosci Biobehav Rev*. 37:2737–2750.

Lisman J. 2017. Glutamatergic synapses are structurally and biochemically complex because of multiple plasticity processes: long-term potentiation, long-term depression, short-term potentiation and scaling. *Philos Trans R Soc Lond B Biol Sci*. 372:20160260.

Lisman JE, Harris KM. 1993. Quantal analysis and synaptic anatomy—integrating two views of hippocampal plasticity. *Trends Neurosci*. 16:141–147.

Lo L, Anderson DJ. 2011. A Cre-dependent, anterograde transsynaptic viral tracer for mapping output pathways of genetically marked neurons. *Neuron*. 72:938–950.

Luo P, Li A, Zheng Y, Han Y, Tian J, Xu Z, Gong H, Li X. 2019. Whole brain mapping of long-range direct input to glutamatergic and GABAergic neurons in motor cortex. *Front Neuroanat*. 13:44.

Luscher C, Nicoll RA, Malenka RC, Muller D. 2000. Synaptic plasticity and dynamic modulation of the postsynaptic membrane. *Nat Neurosci*. 3:545–550.

MacDonald V, Halliday GM. 2002. Selective loss of pyramidal neurons in the pre-supplementary motor cortex in Parkinson's disease. *Mov Disord*. 17:1166–1173.

Mallet N, Delgado L, Chazalon M, Miguelez C, Baufreton J. 2019. Cellular and synaptic dysfunctions in Parkinson's disease: stepping out of the striatum. *Cell*. 8:1005.

Masilamoni G, Votaw J, Howell L, Villalba RM, Goodman M, Voll RJ, Stehouwer J, Wichmann T, Smith Y. 2010. (18)F-FECNT: validation as PET dopamine transporter ligand in parkinsonism. *Exp Neurol*. 226:265–273.

Masilamoni GJ, Bogenpohl JW, Alagille D, Delevich K, Tamagnan G, Votaw JR, Wichmann T, Smith Y. 2011. Metabotropic glutamate receptor 5 antagonist protects dopaminergic and noradrenergic neurons from degeneration in MPTP-treated monkeys. *Brain*. 134:2057–2073.

Masilamoni GJ, Smith Y. 2018. Chronic MPTP administration regimen in monkeys: a model of dopaminergic and non-dopaminergic cell loss in Parkinson's disease. *J Neural Transm (Vienna)*. 125:337–363.

Matelli M, Luppino G. 1996. Thalamic input to mesial and superior area 6 in the macaque monkey. *J Comp Neurol*. 372:59–87.

Matelli M, Luppino G, Fogassi L, Rizzolatti G. 1989. Thalamic input to inferior area 6 and area 4 in the macaque monkey. *J Comp Neurol*. 280:468–488.

Mathai A, Ma Y, Pare JF, Villalba RM, Wichmann T, Smith Y. 2015. Reduced cortical innervation of the subthalamic nucleus in MPTP-treated parkinsonian monkeys. *Brain*. 138:946–962.

Matsumoto N, Minamimoto T, Graybiel AM, Kimura M. 2001. Neurons in the thalamic CM-Pf complex supply striatal neurons with information about behaviorally significant sensory events. *J Neurophysiol*. 85:960–976.

Matsuzaka Y, Aizawa H, Tanji J. 1992. A motor area rostral to the supplementary motor area (presupplementary motor area) in the monkey: neuronal activity during a learned motor task. *J Neurophysiol*. 68:653–662.

McFarland NR, Haber SN. 2002. Thalamic relay nuclei of the basal ganglia form both reciprocal and nonreciprocal cortical connections, linking multiple frontal cortical areas. *J Neurosci*. 22:8117–8132.

Melief EJ, McKinley JW, Lam JY, Whiteley NM, Gibson AW, Neumaier JF, Henschen CW, Palmiter RD, Bamford NS, Darvas M. 2018. Loss of glutamate signaling from the thalamus to dorsal striatum impairs motor function and slows the execution of learned behaviors. *NPJ Parkinsons Dis*. 4: 23.

Meshul CK, Cogen JP, Cheng HW, Moore C, Krentz L, McNeill TH. 2000. Alterations in rat striatal glutamate synapses following a lesion of the cortico- and/or nigrostriatal pathway. *Exp Neurol*. 165:191–206.

Meshul CK, Emre N, Nakamura CM, Allen C, Donohue MK, Buckman JF. 1999. Time-dependent changes in striatal glutamate synapses following a 6-hydroxydopamine lesion. *Neuroscience*. 88:1–16.

Mitchell BD, Cauller LJ. 2001. Corticocortical and thalamocortical projections to layer I of the frontal neocortex in rats. *Brain Res*. 921:68–77.

Morel A, Liu J, Wannier T, Jeanmonod D, Rouiller EM. 2005. Divergence and convergence of thalamocortical projections to premotor and supplementary motor cortex: a multiple tracing study in the macaque monkey. *Eur J Neurosci*. 21: 1007–1029.

Nahmani M, Erisir A. 2005. vGluT2 immunochemistry identifies thalamocortical terminals in layer 4 of adult and developing visual cortex. *J Comp Neurol*. 484:458–473.

Nakamura K, Sakai K, Hikosaka O. 1998. Neuronal activity in medial frontal cortex during learning of sequential procedures. *J Neurophysiol*. 80:2671–2687.

Nakamura K, Sakai K, Hikosaka O. 1999. Effects of local inactivation of monkey medial frontal cortex in learning of sequential procedures. *J Neurophysiol*. 82:1063–1068.

Nakano K, Tokushige A, Kohno M, Hasegawa Y, Kayahara T, Sasaki K. 1992. An autoradiographic study of cortical projections from motor thalamic nuclei in the macaque monkey. *Neurosci Res*. 13:119–137.

Nambu A, Yoshida S, Jinnai K. 1988. Projection on the motor cortex of thalamic neurons with pallidal input in the monkey. *Exp Brain Res*. 71:658–662.

Nambu A, Yoshida S, Jinnai K. 1991. Movement-related activity of thalamic neurons with input from the globus pallidus and projection to the motor cortex in the monkey. *Exp Brain Res*. 84:279–284.

Neuhoff H, Roeper J, Schweizer M. 1999. Activity-dependent formation of perforated synapses in cultured hippocampal neurons. *Eur J Neurosci*. 11:4241–4250.

Nieto-Sampedro M, Lewis ER, Cotman CW, Manthorpe M, Skaper SD, Barbin G, Longo FM, Varon S. 1982. Brain injury causes a time-dependent increase in neuronotrophic activity at the lesion site. *Science*. 217:860–861.

Obeso JA, Marin C, Rodriguez-Oroz C, Blesa J, Benitez-Temino B, Mena-Segovia J, Rodriguez M, Olanow CW. 2008. The basal ganglia in Parkinson's disease: current concepts and unexplained observations. *Ann Neurol*. 64(Suppl 2):S30–S46.

Obeso JA, Rodriguez-Oroz MC, Rodriguez M, Lanciego JL, Artieda J, Gonzalo N, Olanow CW. 2000. Pathophysiology of the basal ganglia in Parkinson's disease. *Trends Neurosci*. 23:S8–S19.

Oda S, Funato H, Sato F, Adachi-Akahane S, Ito M, Takase K, Kuroda M. 2014. A subset of thalamocortical projections to the retrosplenial cortex possesses two vesicular glutamate transporter isoforms, vGluT1 and vGluT2, in axon terminals and somata. *J Comp Neurol*. 522:2089–2106.

Parent M, Parent A. 2005. Single-axon tracing and three-dimensional reconstruction of Centre median-parafascicular thalamic neurons in primates. *J Comp Neurol*. 481:127–144.

Parr-Brownlie LC, Hyland BI. 2005. Bradykinesia induced by dopamine D2 receptor blockade is associated with reduced motor cortex activity in the rat. *J Neurosci*. 25:5700–5709.

Pasquereau B, DeLong MR, Turner RS. 2016. Primary motor cortex of the parkinsonian monkey: altered encoding of active movement. *Brain*. 139:127–143.

Pasquereau B, Turner RS. 2011. Primary motor cortex of the parkinsonian monkey: differential effects on the spontaneous activity of pyramidal tract-type neurons. *Cereb Cortex*. 21:1362–1378.

Pasquereau B, Turner RS. 2013. Primary motor cortex of the parkinsonian monkey: altered neuronal responses to muscle stretch. *Front Syst Neurosci*. 7:98.

Pelled G, Bergman H, Goelman G. 2002. Bilateral overactivation of the sensorimotor cortex in the unilateral rodent model of Parkinson's disease—a functional magnetic resonance imaging study. *Eur J Neurosci*. 15:389–394.

Pellizzer G, Sargent P, Georgopoulos AP. 1995. Motor cortical activity in a context-recall task. *Science*. 269:702–705.

Picard N, Strick PL. 2001. Imaging the premotor areas. *Curr Opin Neurobiol*. 11:663–672.

Przedborski S, Jackson-Lewis V, Djaldetti R, Liberatore G, Vila M, Vukosavic S, Almer G. 2000. The parkinsonian toxin MPTP: action and mechanism. *Restor Neurol Neurosci*. 16:135–142.

Raju DV, Ahern TH, Shah DJ, Wright TM, Standaert DG, Hall RA, Smith Y. 2008. Differential synaptic plasticity of the corticostriatal and thalamostriatal systems in an MPTP-treated monkey model of parkinsonism. *Eur J Neurosci*. 27:1647–1658.

Raju DV, Shah DJ, Wright TM, Hall RA, Smith Y. 2006. Differential synaptology of vGluT2-containing thalamostriatal afferents between the patch and matrix compartments in rats. *J Comp Neurol*. 499:231–243.

Rascol O, Sabatini U, Chollet F, Celsis P, Montastruc JL, Marc-Vergnes JP, Rascol A. 1992. Supplementary and primary sensory motor area activity in Parkinson's disease. Regional cerebral blood flow changes during finger movements and effects of apomorphine. *Arch Neurol*. 49:144–148.

Rizzolatti G, Fadiga L, Gallese V, Fogassi L. 1996. Premotor cortex and the recognition of motor actions. *Brain Res Cogn Brain Res*. 3:131–141.

Rodriguez-Moreno J, Porrero C, Rollenhagen A, Rubio-Teves M, Casas-Torremocha D, Alonso-Nanclares L, Yakoubi R, Santuy A, Merchan-Perez A, DeFelipe J, et al. 2020. Area-specific synapse structure in branched posterior nucleus axons reveals a new level of complexity in thalamocortical networks. *J Neurosci*. 40:2663–2679.

Roland PE, Larsen B, Lassen NA, Skinhoj E. 1980. Supplementary motor area and other cortical areas in organization of voluntary movements in man. *J Neurophysiol*. 43:118–136.

Rouiller EM, Liang F, Babalian A, Moret V, Wiesendanger M. 1994. Cerebellothalamocortical and pallidothalamocortical projections to the primary and supplementary motor cortical areas: a multiple tracing study in macaque monkeys. *J Comp Neurol*. 345:185–213.

Rouiller EM, Tanne J, Moret V, Boussaoud D. 1999. Origin of thalamic inputs to the primary, premotor, and supplementary motor cortical areas and to area 46 in macaque monkeys: a multiple retrograde tracing study. *J Comp Neurol*. 409:131–152.

Rubio-Garrido P, Perez-de-Manzo F, Porrero C, Galazo MJ, Clasca F. 2009. Thalamic input to distal apical dendrites in neocortical layer 1 is massive and highly convergent. *Cereb Cortex*. 19:2380–2395.

Sabatini U, Boulanouar K, Fabre N, Martin F, Carel C, Colonnese C, Bozzao L, Berry I, Montastruc JL, Chollet F, et al. 2000. Cortical motor reorganization in akinetic patients with Parkinson's disease: a functional MRI study. *Brain*. 123:394–403.

Sato F, Nakamura Y, Shinoda Y. 1997. Serial electron microscopic reconstruction of axon terminals on physiologically identified thalamocortical neurons in the cat ventral lateral nucleus. *J Comp Neurol*. 388:613–631.

Schirinzi T, Madeo G, Martella G, Maltese M, Picconi B, Calabresi P, Pisani A. 2016. Early synaptic dysfunction in Parkinson's disease: insights from animal models. *Mov Disord*. 31:802–813.

Seiss E, Praamstra P. 2004. The basal ganglia and inhibitory mechanisms in response selection: evidence from subliminal priming of motor responses in Parkinson's disease. *Brain*. 127:330–339.

Sherwood CC, Raghanti MA, Stimpson CD, Spocter MA, Uddin M, Boddy AM, Wildman DE, Bonar CJ, Lewandowski AH, Phillips KA, et al. 2010. Inhibitory interneurons of the human prefrontal cortex display conserved evolution of the phenotype and related genes. *Proc Biol Sci*. 277:1011–1020.

Shima K, Aya K, Mushiake H, Inase M, Aizawa H, Tanji J. 1991. Two movement-related foci in the primate cingulate cortex observed in signal-triggered and self-paced forelimb movements. *J Neurophysiol*. 65:188–202.

Shima K, Tanji J. 1998. Both supplementary and presupplementary motor areas are crucial for the temporal organization of multiple movements. *J Neurophysiol*. 80:3247–3260.

Shindo K, Shima K, Tanji J. 1995. Spatial distribution of thalamic projections to the supplementary motor area and the primary motor cortex: a retrograde multiple labeling study in the macaque monkey. *J Comp Neurol*. 357:98–116.

Singer TP, Ramsay RR, McKeown K, Trevor A, Castagnoli NE Jr. 1988. Mechanism of the neurotoxicity of 1-methyl-4-phenylpyridinium (MPP+), the toxic bioactivation product of 1-methyl-4-phenyl-1,2,3,6-tetrahydropyridine (MPTP). *Toxicology*. 49:17–23.

Smith Y, Bevan MD, Shink E, Bolam JP. 1998. Microcircuitry of the direct and indirect pathways of the basal ganglia. *Neuroscience*. 86:353–387.

Smith Y, Galvan A, Ellender TJ, Doig N, Villalba RM, Huerta-Ocampo I, Wichmann T, Bolam JP. 2014. The thalamostriatal system in normal and diseased states. *Front Syst Neurosci*. 8:5.

Smith Y, Surmeier DJ, Redgrave P, Kimura M. 2011. Thalamic contributions to basal ganglia-related behavioral switching and reinforcement. *J Neurosci*. 31:16102–16106.

Smith Y, Villalba RM, Raju DV. 2009. Striatal spine plasticity in Parkinson's disease: pathological or not? *Parkinsonism Relat Disord*. 15(Suppl 3):S156–S161.

Smith Y, Wichmann T, Factor SA, DeLong MR. 2012. Parkinson's disease therapeutics: new developments and challenges since the introduction of levodopa. *Neuropsychopharmacology*. 37:213–246.

Smith Y, Villalba RM, Pare JF, Wichmann T. 2013. Dendritic spine pathology in the primary motor cortex (M1) of MPTP-treated parkinsonian monkeys. *Soc Neurosci Abstr*. Program No 240.01. On line.

Sorra KE, Harris KM. 2000. Overview on the structure, composition, function, development, and plasticity of hippocampal dendritic spines. *Hippocampus*. 10:501–511.

Stephens B, Mueller AJ, Shering AF, Hood SH, Taggart P, Arbuthnott GW, Bell JE, Kilford L, Kingsbury AE, Daniel SE, et al. 2005. Evidence of a breakdown of corticostriatal connections in Parkinson's disease. *Neuroscience*. 132:741–754.

Stepniewska I, Preuss TM, Kaas JH. 1994. Thalamic connections of the primary motor cortex (M1) of owl monkeys. *J Comp Neurol*. 349:558–582.

Stepniewska I, Preuss TM, Kaas JH. 2007. Thalamic connections of the dorsal and ventral premotor areas in new world owl monkeys. *Neuroscience*. 147:727–745.

Swain AJ, Galvan A, Wichmann T, Smith Y. 2020. Structural plasticity of GABAergic and glutamatergic networks in the motor thalamus of parkinsonian monkeys. *J Comp Neurol*. 528:1436–1456.

Tanaka KF, Matsui K, Sasaki T, Sano H, Sugio S, Fan K, Hen R, Nakai J, Yanagawa Y, Hasuwa H, et al. 2012. Expanding the repertoire of optogenetically targeted cells with an enhanced gene expression system. *Cell Rep*. 2:397–406.

Taniwaki T, Yoshiura T, Ogata K, Togao O, Yamashita K, Kida H, Miura S, Kira J, Tobimatsu S. 2013. Disrupted connectivity of motor loops in Parkinson's disease during self-initiated but not externally-triggered movements. *Brain Res*. 1512:45–59.

Tanji J, Shima K. 1994. Role for supplementary motor area cells in planning several movements ahead. *Nature*. 371:413–416.

Turner RS, DeLong MR. 2000. Corticostriatal activity in primary motor cortex of the macaque. *J Neurosci*. 20:7096–7108.

Turner RS, Grafton ST, McIntosh AR, DeLong MR, Hoffman JM. 2003. The functional anatomy of parkinsonian bradykinesia. *Neuroimage*. 19:163–179.

van Nuland AJM, den Ouden HEM, Zach H, Dirkx MFM, van Asten JJA, Scheenen TWJ, Toni I, Cools R, Helmich RC. 2020. GABAergic changes in the thalamocortical circuit in Parkinson's disease. *Hum Brain Mapp*. 41:1017–1029.

Varoqui H, Schafer MK, Zhu H, Weihe E, Erickson JD. 2002. Identification of the differentiation-associated Na+/PI transporter as a novel vesicular glutamate transporter expressed in a distinct set of glutamatergic synapses. *J Neurosci*. 22:142–155.

Vigneault E, Poirel O, Riad M, Prud'homme J, Dumas S, Turecki G, Fasano C, Mechawar N, El Mestikawy S. 2015. Distribution of vesicular glutamate transporters in the human brain. *Front Neuroanat*. 9:23.

Villalba RM, Lee H, Smith Y. 2009. Dopaminergic denervation and spine loss in the striatum of MPTP-treated monkeys. *Exp Neurol*. 215:220–227.

Villalba RM, Smith Y. 2010. Striatal spine plasticity in Parkinson's disease. *Front Neuroanat*. 4:133.

Villalba RM, Smith Y. 2011. Differential structural plasticity of corticostriatal and thalamostriatal axo-spinous synapses in MPTP-treated parkinsonian monkeys. *J Comp Neurol*. 519:989–1005.

Villalba RM, Smith Y. 2013. Differential striatal spine pathology in Parkinson's disease and cocaine addiction: a key role of dopamine? *Neuroscience*. 251:2–20.

Villalba RM, Wichmann T, Smith Y. 2014a. Neuronal loss in the caudal intralaminar thalamic nuclei in a primate model of Parkinson's disease. *Brain Struct Funct*. 219:381–394.

Villalba RM, Pare JF, Wichmann T, Smith Y. 2014b. Loss of glutamatergic thalamic input (vGluT2-positive) in deep layers of primary motor cortex (M1) of MPTP-treated parkinsonian monkeys. *Soc Neurosci Abstr*. Program No 248.11. On line.

Villalba RM, Mathai A, Smith Y. 2015. Morphological changes of glutamatergic synapses in animal models of Parkinson's disease. *Front Neuroanat*. 9:117.

Villalba RM, Pare JF, Smith Y. 2016. Three-dimensional electron microscopy imaging of spines in non-human primates. In: Bocstale EJV, editor. *Transmission electron microscopy methods for understanding the brain*. New York (NY): Humana Press, Springer Protocols, pp. p81–p103.

Villalba RM, Smith Y. 2018. Loss and remodeling of striatal dendritic spines in Parkinson's disease: from homeostasis to maladaptive plasticity? *J Neural Transm (Vienna)*. 125:431–447.

Villalba RM, Pare JF, Smith Y. 2018. Differential ultrastructural reorganization of thalamo-cortical and cortico-cortical glutamatergic innervation in the primary motor cortex of MPTP-treated parkinsonian non-human primates. *Soc Neurosci Abstr*.Program No 655.25. Online.

Villalba RM, Pare JF, Lee S, Lee S, Smith Y. 2019. Thalamic degeneration in MPTP-treated Parkinsonian monkeys: impact upon glutamatergic innervation of striatal cholinergic interneurons. *Brain Struct Funct*. 224:3321–3338.

Watanabe Y, Himeda T, Araki T. 2005. Mechanisms of MPTP toxicity and their implications for therapy of Parkinson's disease. *Med Sci Monit*. 11:RA17–RA23.

Wichmann T, DeLong MR. 1996. Functional and pathophysiological models of the basal ganglia. *Curr Opin Neurobiol*. 6:751–758.

Wichmann T, DeLong MR. 1998. Models of basal ganglia function and pathophysiology of movement disorders. *Neurosurg Clin N Am*. 9:223–236.

Wichmann T, DeLong MR. 1999. Oscillations in the basal ganglia. *Nature*. 400:621–622.

Wichmann T, DeLong MR. 2003. Pathophysiology of Parkinson's disease: the MPTP primate model of the human disorder. *Ann N Y Acad Sci*. 991:199–213.

Wichmann T, DeLong MR. 2006. Basal ganglia discharge abnormalities in Parkinson's disease. *J Neural Transm Suppl*. 70:21–25.

Wichmann T, Delong MR. 2007. Anatomy and physiology of the basal ganglia: relevance to Parkinson's disease and related disorders. *Handb Clin Neurol*. 83:1–18.

Wichmann T, DeLong MR, Guridi J, Obeso JA. 2011. Milestones in research on the pathophysiology of Parkinson's disease. *Mov Disord*. 26:1032–1041.

Wichmann T, Dostrovsky JO. 2011. Pathological basal ganglia activity in movement disorders. *Neuroscience*. 198: 232–244.

Wiesendanger R, Wiesendanger M. 1985. The thalamic connections with medial area 6 (supplementary motor cortex) in the monkey (macaca fascicularis). *Exp Brain Res*. 59: 91–104.

Xu T, Wang S, Lalchandani RR, Ding JB. 2017. Motor learning in animal models of Parkinson's disease: aberrant synaptic plasticity in the motor cortex. *Mov Disord*. 32:487–497.

Yamamoto T, Kishimoto Y, Yoshikawa H, Oka H. 1990. Cortical laminar distribution of rat thalamic ventrolateral fibers demonstrated by the PHA-L anterograde labeling method. *Neurosci Res*. 9:148–154.

Yamawaki N, Borges K, Suter BA, Harris KD, Shepherd GM. 2014. A genuine layer 4 in motor cortex with prototypical synaptic circuit connectivity. *Elife*. 3:e05422.

Yamawaki N, Shepherd GM. 2015. Synaptic circuit organization of motor corticothalamic neurons. *J Neurosci*. 35:2293–2307.

Young NA, Collins CE, Kaas JH. 2013. Cell and neuron densities in the primary motor cortex of primates. *Front Neural Circuits*. 7:30.

Zaja-Milatovic S, Milatovic D, Schantz AM, Zhang J, Montine KS, Samii A, Deutch AY, Montine TJ. 2005. Dendritic degeneration in neostriatal medium spiny neurons in Parkinson disease. *Neurology*. 64:545–547.

Zecevic N, Bourgeois J-P, Rakic P. 1989. Changes in synaptic density in motor cortex of rhesus monkey during fetal and postnatal life. *Dev Brain Res*. 50:11–32.

Zheng X, Huang Z, Zhu Y, Liu B, Chen Z, Chen T, Jia L, Li Y, Lei W. 2019. Increase in glutamatergic terminals in the striatum following dopamine depletion in a rat model of Parkinson's disease. *Neurochem Res*. 44:1079–1089.